Title
An extended amygdala-midbrain circuit controlling cocaine withdrawal-induced anxiety and reinstatement

Journal
Cell Reports, 39(5)

ISSN
2639-1856

Authors
Tian, Guilian
Hui, May
Macchia, Desiree
et al.

Publication Date
2022-05-01

DOI
10.1016/j.celrep.2022.110775

HHS Public Access

Author manuscript

Cell Rep. Author manuscript; available in PMC 2022 June 23.

Published in final edited form as:

Cell Rep. 2022 May 03; 39(5): 110775. doi:10.1016/j.celrep.2022.110775.

An extended amygdala-midbrain circuit controlling cocaine withdrawal-induced anxiety and reinstatement

Guilian Tian[1],

May Hui[1],

Desiree Macchia[1],

Pieter Derdeyn[2],

Alexandra Rogers[3],

Elizabeth Hubbard[1],

Chengfeng Liu[1],

Jose J. Vasquez[1],

Lara Taniguchi[3],

Katrina Bartas[2],

Sean Carroll[1],

Kevin T. Beier[1,4,5,6,7,8,9,*]

[1]Department of Physiology and Biophysics, University of California, Irvine, Irvine, CA 92617, USA

[2]Program in Mathematical, Computational, and Systems Biology, University of California, Irvine, Irvine, CA 92617, USA

[3]Interdepartmental Neuroscience Program, University of California, Irvine, Irvine, CA 92617, USA

[4]Department of Pharmaceutical Sciences, University of California, Irvine, Irvine, CA 92617, USA

[5]Department of Biomedical Engineering, University of California, Irvine, Irvine, CA 92617, USA

[6]Department of Neurobiology and Behavior, University of California, Irvine, Irvine, CA 92617, USA

*Correspondence: kbeier@uci.edu.

AUTHOR CONTRIBUTIONS

K.T.B. designed the study. K.T.B. and G.T. performed the experiments. M.H., D.M., A.R., E.H., J.J.V., and S.C. assisted with performing experiments. P.D. and K.B. helped to analyze the data. K.T.B. wrote the paper with input from G.T., M.H., D.M., P.D., A.R., and E.H.

SUPPLEMENTAL INFORMATION

Supplemental information can be found online at https://doi.org/10.1016/j.celrep.2022.110775.

DECLARATION OF INTERESTS

The authors declare no competing interests.

INCLUSION AND DIVERSITY

One or more of the authors of this paper self-identifies as a member of the LGBTQ+ community. One or more of the authors of this paper self-identifies as an underrepresented ethnic minority in science. One or more of the authors of this paper received support from a program designed to increase minority representation in science. While citing references scientifically relevant for this work, we also actively worked to promote gender balance in our reference list.

[7]Center for the Neurobiology of Learning and Memory, University of California, Irvine, Irvine, CA 92617, USA

[8]UCI Mind, University of California, Irvine, Irvine, CA 92617, USA

[9]Lead contact

SUMMARY

Although midbrain dopamine (DA) circuits are central to motivated behaviors, our knowledge of how experience modifies these circuits to facilitate subsequent behavioral adaptations is limited. Here we demonstrate the selective role of a ventral tegmental area DA projection to the amygdala (VTA^{DA}→amygdala) for cocaine-induced anxiety but not cocaine reward or sensitization. Our rabies virus-mediated circuit mapping approach reveals a persistent elevation in spontaneous and task-related activity of inhibitory GABAergic cells from the bed nucleus of the *stria terminalis* (BNST) and downstream VTA^{DA}→amygdala cells that can be detected even after a single cocaine exposure. Activity in $BNST^{GABA}$→midbrain cells is related to cocaine-induced anxiety but not reward or sensitization, and silencing this projection prevents development of anxiety during protracted withdrawal after cocaine administration. Finally, we observe that VTA^{DA}→amygdala cells are strongly activated after a challenge exposure to cocaine and that activity in these cells is necessary and sufficient for reinstatement of cocaine place preference.

Graphical abstract

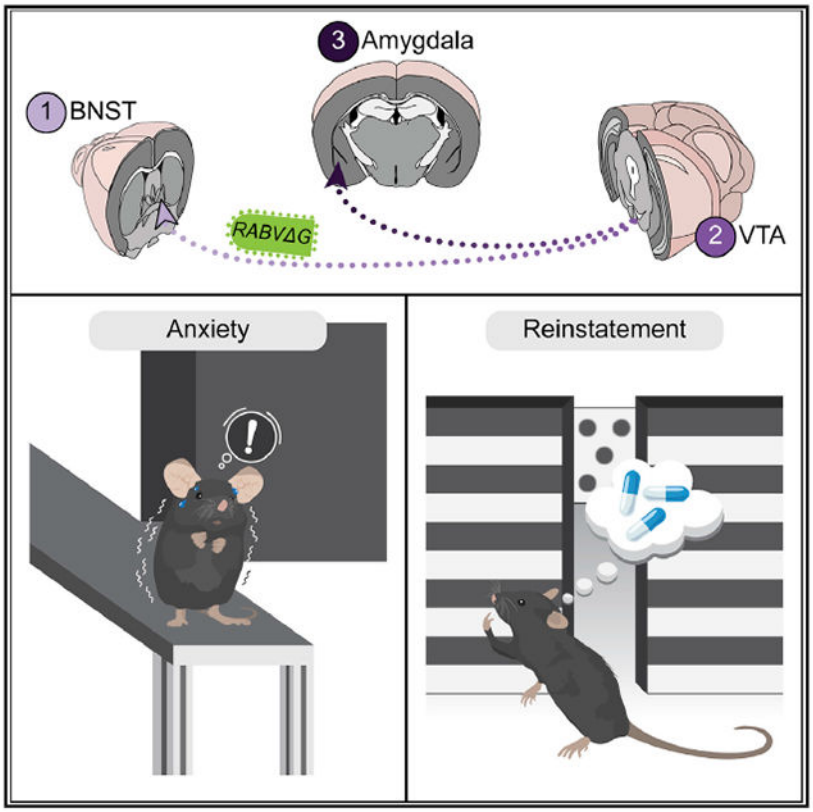

In brief

Tian et al. show that an elevation of $BNST^{GABA}\rightarrow$midbrain cell activity is related to withdrawal anxiety that manifests after a single cocaine exposure. Inhibition or activation of the $BNST^{GABA}\rightarrow VTA^{DA}\rightarrow$amygdala pathway bidirectionally controls cocaine-induced withdrawal anxiety. Activation of $VTA^{DA}\rightarrow$amygdala cells is also sufficient to drive robust reinstatement of cocaine-induced place preference.

INTRODUCTION

Midbrain dopamine (DA) cells and their target structures, such as the nucleus accumbens (NAc) and medial prefrontal cortex (mPFC) have been critically implicated in development and maintenance of drug addiction. Addiction occurs in phases: initial drug exposures are rewarding, repeated administration leads to tolerance or sensitization to the drug's effects, and withdrawal leads to anxiety and a negative affective state, which, in turn, contribute to reinstatement of drug taking/seeking (Sanchis-Segura and Spanagel, 2006). Each of these adaptations is dependent on midbrain DA cells (Coque et al., 2011; Dong et al., 2004), likely through induction of DA-dependent plasticity in target brain structures (Mameli et al., 2009). Recent studies have demonstrated that DA cells are heterogeneous in their transcriptional and electrophysiological profiles, behavioral functions, projection sites, and input patterns (Bromberg-Martin et al., 2010; Lammel et al., 2014; Schultz, 2007). Therefore, to understand how drug use and withdrawal contribute to long-lasting changes in animal behavior, a more nuanced picture of how select midbrain DA cells contribute to specific aspects of behavioral adaptation is needed.

Although the majority of addiction research has been focused on how drug-evoked DA release in the NAc contributes to drug reward (Di Chiara et al., 2004; Koob and Le Moal, 2001; Nestler, 2005; Volkow et al., 2004; Wise, 2004), DA is involved in a wide array of other addiction-related processes. For example, withdrawal from drug use triggers an anxiety state mediated by the extended amygdala that, in turn, contributes to relapse (Aston-Jones and Harris, 2004). Elevations in DA neuron activity have been shown to be linked to anxiety, as infusion of DA Drd2 receptor antagonists into the VTA and amygdala attenuates anxiety (Oliveira et al., 2009; de Oliveira et al., 2011), and elevations in DA cell activity appear to induce anxiety (Coque et al., 2011). These results point to the potential requirement of activation of $VTA^{DA}\rightarrow$amygdala cells for development and expression of anxiety-related behaviors. However, a more recent study found that inhibition of $VTA^{DA}\rightarrow$amygdala cells, as may occur after nicotine administration, induces anxiety (Nguyen et al., 2021). Therefore, the role of $VTA^{DA}\rightarrow$amygdala cells in development of anxiety states, such as those induced during withdrawal from repeated drug use, is controversial. Notably, the negative affective state that includes anxiety occurs in parallel with defects in other DA-dependent processes. For example, reward processing in the mesolimbic DA system is disrupted during protracted withdrawal (Dole et al., 1966; Koob and Le Moal, 1997; Martin and Jasinski, 1969). Although these adaptations have typically been thought to be independent, it is possible that they may, in fact, be linked. However, the potential circuit substrates that may orchestrate parallel adaptations in anxiety and reward processing, such as those related to withdrawal and reinstatement, are not known.

DA is ideally positioned to facilitate these adaptations in response to drug administration and withdrawal. DA is critical for reward- and aversion-related behavior (Bromberg-Martin et al., 2010; Lammel et al., 2012; Wise, 2004), and modifications to VTA^{DA} cells enables processing of positive and negative reinforcements to enact adaptation to a dynamic environment (Lüscher and Malenka, 2011; Pignatelli and Bonci, 2015). Although the contribution of DA cells to reward and aversion learning is relatively well understood, our knowledge of how experience modifies the functional properties of these cells to facilitate learning is incomplete. In addition to DA cells, the identity of input populations that control activation of specific midbrain DA cell populations and how they are modified by experience is not clear. The recent advent of the monosynaptic rabies virus (RABV) circuit mapping strategy has enabled dissection of input cell contributions to behavior as well as a greater understanding of how selected input populations influence defined DA cell populations (Beier et al., 2015; Lammel et al., 2012; Lerner et al., 2015; Menegas et al., 2018; Tian et al., 2016). However, much remains to be understood about how input populations contribute to DA-dependent learning in a broad range of reward- and aversion-related behaviors, including those elicited by drugs of abuse.

Here we demonstrate that $VTA^{DA}\rightarrow$amygdala cells are critical for development of cocaine withdrawal-induced anxiety and reinstatement. Activity of these cells during cocaine exposure was required for the subsequent development of anxiety during protracted withdrawal after repeated cocaine administration. We then used RABV-mediated circuit mapping, calcium imaging, and chemogenetic inhibition in defined cell types and projections to demonstrate that $BNST^{GABA}$ cells control development of anxiety states through their projections to the midbrain via $VTA^{DA}\rightarrow$amygdala cells. Finally, we found that activity in $VTA^{DA}\rightarrow$amygdala cells is necessary and sufficient for reinstatement of cocaine-induced conditioned place preference (CPP), demonstrating that the same pathway underlies withdrawal anxiety and reinstatement.

RESULTS

Activity in $VTA^{DA}\rightarrow$amygdala cells is selectively required for cocaine-induced anxiety

We first wanted to identify which midbrain DA cells were responsible for development of anxiety that occurs during protracted withdrawal after repeated cocaine administration. We therefore silenced activity of unique midbrain DA cells delineated by projection to one of five projection sites: the medial shell of the NAc (NAcMed), lateral shell of the NAc (NAcLat), dorsolateral striatum (DLS), mPFC, and amygdala. To target each cell population, *CAV-FLEx^{loxP}-Flp*, a canine adenovirus that expresses the Flp recombinase in neurons that (1) project to the site where CAV is injected and (2) express the Cre recombinase (Beier et al., 2015; Schwarz et al., 2015), was injected into one of the five forebrain sites. During the same surgery, an adeno-associated virus (AAV) expressing Flp-dependent hM4Di, an inhibitory DREADD (Armbruster et al., 2007), or YFP (*AAV_{DJ}-hSyn-FLEx^{FRT}-hM4Di* or *AAV_{DJ}-EF1α-fDIO-EYFP*) was injected into the VTA or adjacent *substantia nigra pars compacta* SNc (Figures 1A–1C). After allowing 2 weeks for expression of hM4Di or YFP, we began our protocol. To elicit anxiety during the abstinence period, we needed to perform multiple cocaine administrations prior to abstinence. During the cocaine administration

period, we tested for development of cocaine CPP and locomotor sensitization. CPP is a commonly used measure of reward, and locomotor sensitization is a robust behavioral adaptation in rodents that occurs in response to repeated administration of drugs such as cocaine. The mechanisms underlying CPP and locomotor sensitization are thought to contribute to drug-induced pathophysiological motivational states associated with addiction (Robinson and Berridge, 2000, 2001, 2008; Tzschentke, 2007). Two additional control groups were included where animals received injections of AAVs encoding YFP or hM4Di but received saline injections instead of cocaine. Activity in each DA cell population was modulated by intraperitoneal (i.p.) injection of 5 mg/kg clozapine-N-oxide (CNO), which was administered 30 min before cocaine injection (15 mg/kg). All groups received CNO, except for one additional control group that received no CNO (Figure S1 and S2). After 10 days of abstinence, we tested anxiety by the elevated plus maze (EPM) and time spent in the center of the open field (open field test [OFT]). Neither cocaine nor CNO was administered during anxiety tests because we aimed to measure baseline anxiety during protracted withdrawal.

Chemogenetic inhibition of $VTA^{DA}\rightarrow$amygdala cells during cocaine administration prevented development of withdrawal-induced anxiety (YFP cocaine versus hM4Di cocaine, $p = 0.01$; Figures 1D and S2). Inhibition of four other subpopulations of midbrain DA cells had no effect on anxiety (Figures 1E–1H). Interestingly, the effects of $VTA^{DA}\rightarrow$amygdala cell inhibition were specific for development of withdrawal anxiety because inhibition of these cells had no effect on cocaine reward or sensitization (CPP; YFP cocaine versus hM4Di cocaine, $p = 0.65$; sensitization, YFP cocaine versus hM4Di cocaine, $p = 0.91$; Figures 1I and 1J). CNO administration had no effect on locomotion in animals expressing YFP or hM4Di in $VTA^{DA}\rightarrow$amygdala cells (Figure S2K); a single CNO pairing for these animals in the CPP assay did not elicit CPP or conditioned place aversion (CPA) (Figure S2L); and repeated administration of CNO did not trigger long-lasting anxiety phenotypes (Figures S2M and S2N). These control data demonstrate that the anxiety behavior we observed was due to withdrawal after cocaine administration and that CNO application to hM4Di-expressing or YFP-expressing control animals did not have observable behavioral consequences in our assays. These results indicate that $VTA^{DA}\rightarrow$amygdala cell activity is required during cocaine administration for development of anxiety after protracted withdrawal from repeated cocaine administration.

RABV tracing reveals changes in BNST inputs to $VTA^{DA}\rightarrow$amygdala cells

Salient experiences such as cocaine intake can trigger distinct synaptic modifications onto different projection-defined midbrain DA cells (Lammel et al., 2011). The identity of these synapses is not known. Our RABV-mediated strategy enables identification of input cell populations that are modified by experience, including inputs from GABAergic and glutamatergic cells (Beier et al., 2017). Although our previous study mapped cocaine-induced input changes onto all midbrain DA cells irrespective of projection site, here we combined our circuit screen with our intersectional viral-genetic mapping strategy, cell-type-specific tracing of the relationship between inputs and outputs (cTRIO) (Beier et al., 2015; Lerner et al., 2015; Schwarz et al., 2015), to identify which input populations to $VTA^{DA}\rightarrow$amygdala cells were modified by cocaine. Briefly, *CAV-FLEx^{loxP}-Flp* was

injected into the amygdala, and during the same surgery, Flp-dependent AAVs expressing the avian TVA protein tagged to mCherry (TC) and RABV glycoprotein (RABV-G) were injected into the VTA. After waiting 13 days to enable expression of TC and RABV-G, we injected a single dose of cocaine (15 mg/kg) or saline as a control. The next day, an EnvA-pseudotyped, G-deleted, GFP-expressing RABV (RABVΔG) was injected into the VTA. The EnvA glycoprotein binds to TVA and enables infection specifically of TC-expressing cells; therefore, the EnvA-pseudotyped RABVΔG infected only TC-expressing (and RABVG-expressing) cells in the VTA. Although the RABV was G deleted and thus could not spread on its own, RABV-G was supplied in *trans* in the starter cells, enabling the virus to spread to connected input cells. Because the inputs did not express RABV-G, the virus could not spread farther.

To test for cocaine-induced input changes, we quantified RABV-labeled cells in 22 different anatomically defined brain regions that combined make up more than 90% of long-range inputs to VTA^{DA}→amygdala cells (Beier et al., 2015, 2017, 2019). We observed RABV-labeled neurons in each examined brain site in saline- and cocaine-treated animals, the majority of which had quantitatively similar proportions under both conditions. However, we identified a significant increase in labeled inputs from the BNST onto VTA^{DA}→amygdala cells in cocaine-treated animals (saline, 1.76% of inputs; cocaine, 5.54% of inputs; $p = 0.0014$; Figure 2B). This was the only brain region to reach significance and was still significant even when correcting for multiple comparisons (t tests followed by Holm-Bonferroni correction). These changes were specific to cocaine administration because an aversive foot shock stimulus did not produce this increase in input labeling (Figure S3). Interestingly, we did not observe this elevation in BNST input labeling when sampling inputs onto all VTA^{DA} cells (Beier et al., 2017), suggesting that this increase in input labeling was specific to VTA^{DA}→amygdala cells.

Activity in $BNST^{GABA}$ cells is elevated after a single cocaine exposure

We have shown previously that RABV-mediated input labeling is increased in more highly active connections and decreased in less active ones (Beier et al., 2017). We wanted to test whether the elevation of BNST cell labeling observed here was due to changes in BNST cellular activity or another cause, such as a change in the number of synapses from BNST cells in the ventral midbrain. To do this, we first needed to know the identity of BNST cells projecting to the midbrain. Although GABAergic and glutamatergic cells in the BNST synapse onto VTA^{DA} and VTA^{GABA} cells (Jennings et al., 2013), the proportion of these cells that connect to VTA^{DA}→amygdala cells is not known. Therefore we used *in situ* hybridization in cTRIO brains mapping inputs to VTA^{DA}→amygdala cells to test whether RABV-labeled inputs predominately arose from GABAergic or glutamatergic cells in the BNST and whether cocaine altered the proportion of each cell type labeled. We observed that the majority of RABV-labeled BNST cells projecting to VTA^{DA}→amygdala cells were GABAergic (~75%) and that this proportion was approximately the same in saline- and cocaine-treated animals (Figures 3A–3D). Given that GABAergic cells comprised the majority of inputs from the BNST to VTA^{DA}→amygdala cells, we used the *vGAT-Flp* driver line to access these cells.

We first tested whether cocaine altered the number of synapses from BNST^{GABA} cells in the midbrain by injecting *AAV$_{DJ}$-hSyn-FLEx^{FRT}-mGFP-2A-Synaptophysin-mRuby* into the BNST. This allowed us to quantify the number and size of putative synaptic puncta in the midbrain that arose from BNST^{GABA} cells. We observed no detectable difference in synapse number or volume, suggesting that cocaine did not alter the numbers of inputs or gross properties of synapses from these cells in the midbrain (density, saline versus cocaine p = 0.52; volume, saline versus cocaine p = 0.90; Figures 3E–3H). To test whether a single exposure to cocaine caused a long-lasting change in activity of BNST^{GABA} cells, we used fiber photometry to measure the activity of BNST^{GABA} cells 1 day before and 1 day after cocaine administration. We found that spontaneous activity of BNST^{GABA} cells was elevated 24 h after cocaine administration, reflecting the increase in RABV labeling observed after cocaine administration (D1 versus D3, p = 0.04; Figure S4). Although these cells do project to other brain sites, the dominant projection was to the ventral midbrain, in particular the *substantia nigra pars reticulata* (SNr), a brain region primarily composed of GABAergic neurons (Figure S5). To restrict GCaMP expression to BNST^{GABA} cells that projected to the ventral midbrain, we injected a retrograde AAV (Tervo et al., 2016) expressing Flp-dependent Cre into the ventral midbrain of *vGAT-Flp* mice and Cre-dependent GCaMP7f into the BNST. We observed a similar elevation in spontaneous activity of BNST^{GABA}→midbrain cells 1 day after cocaine administration (D1 versus D3, p = 0.018; Figures 3I and 3J), demonstrating that this elevation occurred in midbrain projection-defined BNST^{GABA} cells.

We next wanted to determine how this elevation in BNST^{GABA}→midbrain cell activity relates to activity of downstream VTA^{DA}→amygdala cells. Although we detected the elevation in BNST^{GABA} input labeling by mapping inputs onto VTA^{DA}→amygdala cells (Figure 2B), BNST^{GABA} cells provide synaptic input to midbrain DA and GABA cells, with a preferential input onto GABA cells (Jennings et al., 2013; Kudo et al., 2012). This is consistent with our observation that the dominant midbrain projection of BNST^{GABA} cells is to the SNr and not the VTA or SNc, where the DA cells are located (Figure S5). We thus expected that an elevation of BNST^{GABA}→midbrain cell activity would be accompanied by an increase in VTA^{DA}→amygdala cell activity through disinhibition via local midbrain GABA cells. Indeed, we found that activity in VTA^{DA}→amygdala cells was elevated 1 day after cocaine administration (D1 versus D3, p = 0.01; Figure 3K). These results are consistent with a disinhibitory mechanism and are similar to our previous results with parvalbumin-positive globus pallidus external segment inputs to VTA^{DA} neurons (Beier et al., 2017).

Activity in the BNST^{GABA}→midbrain projection is required for cocaine-induced anxiety

Cocaine leads to elevated activity in BNST^{GABA}→midbrain and VTA^{DA}→amygdala cells (Figures 3J and 3K), and activity in VTA^{DA}→amygdala cells is necessary for anxiety that develops during protracted withdrawal from cocaine exposure (Figure 1D). Given the parallel increases in activity of BNST^{GABA}→midbrain and VTA^{DA}→amygdala cells, we anticipated that inhibiting the BNST^{GABA}→midbrain projection during cocaine administration would also prevent development of anxiety without affecting cocaine reward or sensitization. To test this, we injected *AAV$_{DJ}$-hSyn-FLEx^{FRT}-hM4Di* or *AAV$_{DJ}$-EF1α-*

fDIO-eYFP as a control into the BNST of *vGAT-Flp* mice, waited 6 weeks to enable terminal expression of hM4Di or YFP, and then began behavioral testing. To specifically inhibit the BNST^{GABA}→midbrain projection, we injected slow-release CNO microspheres into the ventral midbrain (Figure 4A; Beier et al., 2017; Stachniak et al., 2014). These microspheres release CNO for about 7 days; therefore, we condensed our protocol to enable administration of all six cocaine injections within this time window (Figure 4B). Inhibition of the BNST^{GABA}→midbrain projection prevented development of anxiety (YFP cocaine versus hM4Di cocaine, p = 0.0089; Figures 4E and S6) during abstinence after repeated cocaine injection with no effect on cocaine reward (YFP cocaine versus hM4Di cocaine, p = 0.095; Figure 4C) or sensitization (YFP cocaine versus hM4Di cocaine, p = 1.0; Figure 4D). This was the same effect as inhibiting VTA^{DA}→amygdala cells during cocaine administration (Figures 1D, 1I, 1J, and S2). These results demonstrate that activity in the BNST^{GABA} →VTA^{DA}→amygdala pathway during cocaine administration is required for development of anxiety that occurs after protracted withdrawal from repeated cocaine administration.

Behavioral changes mediated by BNST^{GABA} neurons are triggered by VTA^{DA}→amygdala neurons

We next wanted to explore what triggered the elevation in BNST^{GABA} cell activity after a single administration of cocaine. Cocaine prevents DA reuptake in DA neurons through blockade of the DA transporter (DAT), causing an increase in extracellular DA (Torres et al., 2003). The transient increase in DA likely contributes to cellular plasticity evoked by cocaine in downstream structures. The *Drd1* and *Drd2* DA receptors are expressed in the BNST (Figure S7). Interestingly, VTA^{DA}→amygdala neurons send collaterals to the BNST and provide an approximately 15-fold larger input to the BNST than all other VTA^{DA} cells combined (Figures 4F–4I). We therefore tested the possibility that VTA^{DA}→amygdala neurons themselves may trigger the activity increase in BNST^{GABA}→ midbrain neurons through collaterals to the BNST and, ultimately, their own long-lasting activity changes. We therefore expressed hM4Di or YFP in VTA^{DA}→amygdala cells, as in Figure 1, and injected slow-release CNO microspheres into the BNST (Figure 4J). We then followed exactly the same behavioral protocol as for Figure 4B. Inhibition of VTA^{DA}→BNST collaterals from VTA^{DA}→amygdala cells prevented development of cocaine-induced withdrawal anxiety (YFP versus hM4Di, p = 0.032; Figure 4M) with no effect on CPP (YFP versus hM4Di, p = 0.39; Figure 4K) or sensitization (YFP versus hM4Di, p = 0.80; Figure 4L), the same effect as inhibiting VTA^{DA}→amygdala cells through i.p. administration of CNO (Figure 1) and inhibition of BNST^{GABA}→midbrain terminals (Figures 4A–4E). These results indicate that VTA^{DA}→amygdala cells indirectly trigger their own elevation in activity by facilitating a long-lasting increase in activity in BNST^{GABA} cells that project back to the midbrain through collaterals these cells have in the BNST.

Activity in the BNST^{GABA}→VTA^{DA}→amygdala pathway provides an anxiety signal

We next wanted to explore the native activity of the BNST^{GABA}→ VTA^{DA}→amygdala pathway and how it relates to reward, sensitization, and anxiety behaviors in awake, behaving animals. We therefore performed fiber photometry experiments by expressing the calcium-dependent fluorescent protein GCaMP in BNST^{GABA}→ midbrain or

VTA^{DA}→amygdala cells and implanting a chronic fiber over the corresponding cell population. We performed a cocaine administration protocol similar to that performed for Figure 1, although no CNO was administered (Figure 5A). We first examined the task-linked activity in each cell population during chamber crossings in the CPP pre-test and post-test, locomotor initiation and cessation, entries into and exits from the center of the open field, and entries into the closed and open arms of the EPM (Figures 5B and 5C). Both cell populations were minimally active during CPP, locomotion, or the OFT and most active during the EPM task (Figures 5B–5D, S8, and S9). Specifically, BNST^{GABA}→midbrain and VTA^{DA}→amygdala cells were more active during open arm entries and less active during closed arm entries, with the peak of BNST^{GABA}→midbrain neuron activity during open and closed arm entries preceding that of VTA^{DA}→amygdala cells (Figures 5B and 5C). BNST^{GABA}→midbrain and VTA^{DA}→amygdala cells had very similar activity profiles across behavioral events, although the EPM was the only test where both cell populations displayed significant task-related activity (peak Z score greater or less than 0.25; Figure S8). These results indicate that activity of both cell populations signals anxiety, such as that experienced by entrance into the open arms of the maze. Accordingly, the magnitude of activity in BNST^{GABA} and VTA^{DA}→amygdala cells during open arm entries for each mouse correlated with time spent in the open arms for that mouse, with the activity of both populations being inversely related to time spent in the open arms (Figures 5E and 5F). Activation or suppression of activity in these cell populations also related to time spent in the center of the open field but not chamber entries in the CPP task or locomotion (Figure S10). These results demonstrate that activity in BNST^{GABA} and VTA^{DA}→amygdala cells signal an anxiety state.

VTA^{DA}→amygdala cell activity is necessary and sufficient for development of experience-driven anxiety states

We next wanted to test whether activity in the BNST^{GABA}→VTA^{DA}→amygdala pathway is critical for development of anxiety elicited by other experiences. We therefore assessed the necessity of activity in VTA^{DA}→amygdala cells for development of anxiety induced by the model opioid morphine as well as chronic exposure to a predator odor, a natural stimulus. A combination of *CAV-FLEx^{loxP}-Flp* and Flp-dependent AAVs expressing YFP or hM4Di was used to target YFP or hM4Di expression to VTA^{DA}→amygdala cells, as performed previously (Figures 1 and 4). Inhibition of VTA^{DA}→amygdala cells during repeated morphine administration had no effect on CPP (YFP versus hM4Di, p = 0.52; Figure 6B) or locomotor behavior induced by morphine (YFP versus hM4Di, p = 0.34; Figure 6C) but prevented development of anxiety during protracted withdrawal (YFP versus hM4Di, p = 0.02; Figure 6D). We then inhibited the same cells in different animals that were chronically exposed to 2,4,5-tri-methylthiazoline (TMT), a constituent of fox urine that is inherently aversive to rodents and elicits anxiety (Rosen et al., 2015). 4 days of TMT exposure for 1 h per day caused long-lasting anxiety in animals injected with YFP relative to animals not exposed to the predator odor (no predator odor versus predator odor, p = 0.04; Figure 6E), and inhibition of VTA^{DA}→amygdala neurons during odor exposure prevented development of TMT-induced anxiety (YFP versus hM4Di, p = 0.03; Figure 6E). These results demonstrate that activity in the VTA^{DA}→amygdala pathway is required for development of anxiety states. To test whether activation of

VTA^{DA}→amygdala cells is sufficient to induce anxiety, we expressed the chemogenetic activator hM3Dq or YFP as a control in VTA^{DA}→amygdala cells and tested the effects of cell activation on CPP, locomotion, and anxiety (Figure 6F). hM3Dq-mediated activation of VTA^{DA}→amygdala cells had no effect on place preference (YFP versus hM3Dq, p = 0.28; Figure 6G) or locomotion (YFP versus hM3Dq, p = 0.40; Figure S11) but induced an acute anxiety state (YFP versus hM3Dq, p = 0.012; Figures 6H and S11), demonstrating that VTA^{DA}→amygdala cell activation is sufficient to produce anxiety. These results indicate that our method can be generally applied to identify key neuronal circuits that contribute to normal and pathological behavioral adaptations.

Activity in VTA^{DA}→amygdala cells is required for cocaine-primed CPP reinstatement

Withdrawal-related anxiety is one of many factors that contribute to reinstatement of drug taking during abstinence, which include re-exposure to drug-paired cues and environmental stressors (Aston-Jones and Harris, 2004; Koob, 2009; Koob et al., 2004). The amygdala is known to play a central role in cued reinstatement of a variety of behaviors, including drugs of abuse (Cahill and McGaugh, 1990; Everitt et al., 2000; Gallagher, 2000; Ledoux, 2000; Meil and See, 1997). Given the relationship between withdrawal anxiety and relapse, we examined the activity of four different midbrain DA cell populations during each cocaine exposure, including a challenge dose of cocaine that was given 1 day after the EPM and OFT tests after 10 days of protracted withdrawal (Figure 7A). Interestingly, we observed a rhythmic burst of activity after cocaine administration in VTA^{DA}→amygdala cells lasting several minutes that was not seen in the other three midbrain DA cell populations examined (Figure 7B). This activity pattern was present in these cells during all cocaine exposures, but the number of events was about three times greater after the challenge dose than any other cocaine exposure (1.43 events per minute for the first 10 min after the challenge dose versus an average of 0.44 events per minute for all other days; Figure 7B). This led us to hypothesize that the elevated activity of these cells may be related to reinstatement behavior. To test this possibility, we inhibited VTA^{DA}→amygdala cells during the cocaine priming dose in a CPP reinstatement task (Figure 7C). *CAV-FLEx^{loxP}-Flp* was injected into the amygdala, and Flp-dependent AAVs expressing hM4Di or YFP were injected into the VTA to inhibit VTA^{DA}→amygdala cells or as a control, respectively, as shown in Figures 1 and 4. Two weeks after virus injection, CPP was established with a single cocaine pairing as before and then extinguished over two sessions by allowing the animals to freely explore both chambers of the CPP apparatus in the absence of cocaine. Three days later, CNO was injected into all animals 30 min prior to an injection of 7.5 mg/kg cocaine. After cocaine was injected, animals were placed into the CPP chamber. Although YFP-expressing VTA^{DA}→amygdala cells reinstated their CPP, reinstatement was blunted by hM4Di-mediated inhibition of VTA^{DA}→amygdala cells (YFP before/after, p = 0.04; hM4Di before/after, p = 0.57; Figure 7D). Activity of VTA^{DA}→amygdala cells during the priming dose is thus required for cocaine-primed reinstatement of CPP. To test whether activation of VTA^{DA}→amygdala cells is sufficient to induce reinstatement, we expressed hM3Dq or YFP in VTA^{DA}→amygdala cells, established and extinguished cocaine CPP, and then injected CNO 30 min before placing the mice in the CPP apparatus (Figure 7E). Although YFP-expressing mice did not show reinstatement behavior, mice expressing hM3Dq robustly reinstated CPP (reinstatement, pre-test = 342 s; post-test, pretest, 120 s; p = 0.04; Figure 7F).

Our results demonstrate that $VTA^{DA}\rightarrow$amygdala cells play a crucial role in orchestrating withdrawal-related anxiety and relapse-related reinstatement.

DISCUSSION

In this study, we defined the role of the $BNST^{GABA}\rightarrow VTA^{DA}\rightarrow$amygdala pathway in development of anxiety elicited by drugs of abuse and natural experiences. The elucidation of how the $BNST^{GABA}\rightarrow VTA^{DA}\rightarrow$amygdala pathway selectively orchestrates development of experience-induced anxiety and cocaine reinstatement illuminates a direct link between midbrain and extended amygdala networks in development of experience-induced anxiety and reinstatement. The BNST is composed of multiple cell types that release glutamate or GABA as well as a constellation of different neuropeptides (Kash et al., 2015). Glutamatergic and GABAergic BNST cells project to the ventral midbrain, although the majority of those synapsing onto VTA cells are believed to be GABAergic (Dong and Swanson, 2004, 2006a, 2006b; Georges and Aston-Jones, 2001, 2002; Jalabert et al., 2009; Jennings et al., 2013; Kudo et al., 2012). Different populations of BNST cells that project to the VTA mediate differing behavioral outcomes depending on cell type and location in the BNST, indicating a complex interaction between the two structures (Jennings et al., 2013; Kim et al., 2013). For example, although activation of the BNST has been shown to regulate CPP at least in part through its projection to the VTA, it is not clear which BNST cells mediate this reward phenotype; previous studies indicated that they likely arise from the anterodorsal aspect of the BNST and are not glutamatergic (Kim et al., 2013; Sartor and Aston-Jones, 2012). In our study, we found that inhibition of terminals in the midbrain from *vGAT-Flp*-expressing cells in the BNST increased CPP, but this effect was not significant (Figure 4C). Many examples of opposing effects mediated by different BNST cells can be found in the literature, suggesting differing effects of neuron types and subregions in the BNST on downstream behavioral consequences.

In addition to CPP, the BNST has long been implicated in mediating negative affective states, including withdrawal from drugs of abuse. For example, noradrenergic projections in the BNST lead to activation of BNST cells during opiate withdrawal, and corticotropin-releasing factor (CRF) mRNA and protein levels are elevated in the BNST during protracted withdrawal (Delfs et al., 2000; Olive et al., 2002; Shalev et al., 2001). Drugs of abuse elicit long-lasting synaptic plasticity in the BNST; a single dose of cocaine elicits potentiation of glutamatergic transmission in the BNST in a CRF- and DA-dependent manner (Kash et al., 2008), and cocaine self-administration increases the intrinsic excitability and AMPAR/NMDAR ratio of different sets of BNST neurons in the dorsal aspect of the BNST (Debacker et al., 2015; Dumont et al., 2005). These are consistent with our results showing an elevated activity of BNST neuron activity. Opioid dependence, as elicited through chronic implant of a morphine pellet, also induces long-term potentiation (LTP) onto different populations of BNST cells (Dumont et al., 2008; Francesconi et al., 2017), suggesting that plasticity onto BNST cell synapses may be a common feature of drugs of abuse, also consistent with our results. CRF may play a key role in this process because it increases the frequency of excitatory glutamatergic post-synaptic currents onto BNST cells that project to the VTA, a process occluded by ethanol withdrawal (Silberman et al., 2013). Because DA activates CRF-releasing cells, this raises the possibility that DA may act to

elevate the activity of BNST→midbrain cells, including $BNST^{GABA}$→midbrain cells, by increasing CRF levels in the BNST (Silberman et al., 2013). This is consistent with our observation that activity in collaterals in the BNST from VTA^{DA}→amygdala cells was required for the behavioral effects mediated by $BNST^{GABA}$ cells (Figure 4). In addition, the BNST appears to be involved in stress-induced reinstatement because inactivation prevented footshock-induced reinstatement of cocaine-seeking behavior (McFarland et al., 2004). Our results are largely consistent with a body of previous literature implicating the BNST in drug withdrawal anxiety/negative affect and reinstatement of drug-seeking behavior. Although we refer to the DA population we studied here as VTA^{DA}→amygdala cells because we defined them by their projection to the amygdala, the principal action of these cells occurred in the BNST, and therefore it is perhaps more appropriate to consider the function of this BNST→VTA^{DA} loop.

Potential direct link between anxiety and CPP reinstatement

Stress or drug cues induce norepinephrine release into the BNST during protracted drug withdrawal, which promotes an anxiety state. This anxiety state, in turn, may enhance the reward value of drugs via a negative reinforcement mechanism because temporarily eliminating the anxiety becomes a key driver of drug seeking (Aston-Jones and Harris, 2004). It has also been hypothesized that hedonic processing is altered during protracted withdrawal (Dole et al., 1966; Koob and Le Moal, 1997; Martin and Jasinski, 1969), likely through adaptations in midbrain DA cells or their inputs, and that these changes may contribute to relapse/reinstatement. Our results demonstrating the critical role of the BNST and extended amygdala more generally are therefore consistent with previous studies. We extend these observations by showing that withdrawal-induced anxiety and hedonic changes that lead to reinstatement of drug-seeking behaviors may be orchestrated by a single pathway. We provide an integrated framework by which the BNST and midbrain DA cells work in concert with the amygdala to orchestrate anxiety and reinstatement behaviors induced by withdrawal after cocaine administration and a priming dose of cocaine, respectively. It is likely that cocaine causes long-lasting changes in brain circuits that are normally mediated by these cell populations and that without this activity, the changes that normally mediate anxiety states do not effectively occur . Our data also highlight that the anxiety that develops after repeated drug exposure is facilitated by circuit elements that are independent of those that mediate drug reward or sensitization, indicating that reward/sensitization and anxiety are driven by different brain circuits.

Role of VTA^{DA}→amygdala cells in anxiety

Several studies have been published in the past few years about the role of midbrain DA→amygdala cells in reward and aversion learning, fear learning, as well as anxiety (Lin et al., 2020; Lutas et al., 2019; Tang et al., 2020). These and other studies mostly suggest that DA release in the amygdala is associated with state-specific gating of salience cues, including opioid reward and aversion, because silencing DA neurons in the dorsal raphe (DR), which project to the central amygdala (CeA) and BNST, blunted the development and expression of conditioned place aversion associated with opioid withdrawal (Lin et al., 2020). However, studies have not assessed the potential role of VTA^{DA}→amygdala cells in drug-induced anxiety and reinstatement. A recent

study that investigated VTA^{DA}→amygdala cells in the context of nicotine administration reported that silencing, not activating, these cells was anxiogenic (Nguyen et al., 2021). Our results contrast with that observation because we demonstrated that activation of VTA^{DA}→amygdala cells is acutely anxiogenic, whereas inhibition prevents development of anxiety states. We also demonstrated that activity in VTA^{DA}→amygdala cells and BNST^{GABA}→midbrain inputs both signal anxiety, as both cells increase their activity in open arm entries of the EPM, and the activity of both cell populations is positively correlated with anxiety. Although the drug used and methods of inhibition and activation differ between these studies, our results integrate with a larger body of work indicating that DA signaling in the amygdala is principally anxiogenic (Coque et al., 2011; Oliveira et al., 2009; de Oliveira et al., 2011).

One-step RABV mapping as a brain-wide screen for experience-dependent changes

We provide further evidence that our RABV mapping platform can be used to identify experience-dependent modifications in neuronal circuits by identifying cell populations that exhibit changes in baseline cellular activity after an experience. Our RABV approach identified a cocaine-induced elevation in BNST^{GABA} cell activity, and inhibition of this projection to the midbrain was sufficient to prevent cocaine-induced anxiety. Interestingly, although anxiety is typically thought to emerge after repeated drug administration, the negative affective state appears even after a single cocaine exposure (Deckers, 2016; Koob and Le Moal, 2001). These results suggest that the RABV technique is sufficiently sensitive to detect early changes in cellular activity relating to negative affect. In addition, although we used cTRIO from VTA^{DA}→amygdala cells to identify cocaine-induced changes in input cell activity, the effect of these input changes on DA cells may not always be direct. It is necessary to consider potential local microcircuit effects because RABV can identify input changes that may influence multiple cell types in the targeted brain region. In this and our previous study, the GABAergic cells we identified using RABV mapping from midbrain DA cells preferentially project onto the GABAergic SNr. This means that elevations of activity from these inputs likely disinhibit midbrain DA cells, leading to an elevation in DA cell activity, as we found here (Figure 3K) and in our previous study (Beier et al., 2017). We believe that our approach is a valuable screening method to enable dissection of the roles of unique circuits in selective behavioral adaptations.

Pharmacological intervention for psychostimulant abuse has remained elusive in part because drugs that target the entire DA system often have many off-target effects, including on the brain's reward system. Elucidation of the selective role of the BNST^{GABA}→VTA^{DA}→amygdala pathway in development of anxiety and CPP reinstatement provides specific cellular substrates outside of the canonical DA reward circuits that could be used as targets for development of addiction therapeutic agents to reduce the negative affect that develops during withdrawal as well as to prevent reinstatement/relapse.

Limitations of the study

Although our study is consistent with a preferential connection from BNST^{GABA} cells onto midbrain GABA cells that then inhibit VTA^{DA}→amygdala cells, this was not

shown directly. This would require an electrophysiological characterization of midbrain connectivity. Although activity in VTA^{DA}→amygdala cells in the BNST appears to be important for development of withdrawal anxiety, it is not clear that DA is involved. This would require inhibiting DA receptors and demonstrating DA-dependent function. We also did not test whether VTA^{DA}→amygdala neurons signal directly to $BNST^{GABA}$ cells that project back to the midbrain or to other cells that then influence $BNST^{GABA}$→midbrain cells. We do not know whether $BNST^{GABA}$→midbrain cells are a homogeneous or heterogeneous population. We also do not yet know the mechanistic underpinning of why RABV input mapping appears to be sensitive to the activity of input populations. Without this knowledge, it is difficult to directly interpret what changes in RABV labeling mean; this currently must be tested using other methods.

STAR★METHODS

RESOURCE AVAILABILITY

Lead contact—Further information and requests for resources and data should be directed to and will be fulfilled by the lead contact, Kevin T. Beier (kbeier@uci.edu).

Materials availability—RABVΔG used in this study will be distributed upon request.

Data and code availability

- Fiber photometry data have been deposited at Zenodo and are publicly available as of the date of publication. Accession numbers are listed in the Key resources table. Microscopy data reported in this paper will be shared by the lead contact upon reasonable request.
- All original code has been deposited at GitHub and is publicly available as of the date of publication. The DOI information is listed in the Key resources table.
- Any additional information required to reanalyze the data reported in this paper is available upon reasonable request.

EXPERIMENTAL MODEL AND SUBJECT DETAILS

Animals—Mice were housed on a 12-hour light–dark cycle with food and water *ad libitum.* Males and females from a C57/BL6 background were used for all experiments in approximately equal proportions. Mice were approximately 3-4 months of age at the time of experiments.

All surgeries were done under isoflurane anesthesia. All procedures complied with the animal care standards set forth by the National Institute of Health and were approved by the University of California, Irvine's Institutional Animal Care and Use Committee (IACUC).

METHOD DETAILS

Stereotaxic surgery—Mice were anesthetized with 3-4% isoflurane and maintained during surgery at 1-1.5% isoflurane. Mice were secured in a stereotaxic apparatus (Stoelting). Under aseptic conditions, guide holes were drilled and viruses were infused into

the target sites using a glass capillary attached to a microinjection pump (WPI, UMP3T). 500 nL of viruses were infused at a rate of 1.6 nL/s. The glass capillary remained in place for 5 min following the infusion to allow for virus diffusion. After infusion, the surgical incision sites were closed with either sutures or Vetbond tissue adhesive (Patterson Veterinary). Vetameg (flunixin, Patterson veterinary) was administered for pain management and topical bacitracin was applied to prevent infection at the incision site.

Coordinates used for viral injections were (relative to bregma, midline, or dorsal brain surface and in mm):

NAcMed: AP +1.55, ML 0.7, DV −4.0;

NAcLat: AP +1.45, ML 1.75, DV −4.0;

DLS: AP +0.25, ML 2.5, DV −3.4;

Amygdala: AP −1.43, ML 2.5, DV −4.5;

mPFC: two injections, one at AP +2.15, ML 0.27, DV −2.1 and another at AP +2.15, ML 0.27, DV −1.6;

BNST: AP +0.1, ML 0.8, DV −4.0;

VTA: AP −3.2, ML 0.4, DV −4.2;

SNc: AP −3.2, ML 1.2, DV −4.2.

The titers of viruses, based on quantitative PCR analysis, were as follows:

AAV_5-CAG-FLEx^{FRT}-TC, 2.6 × 10^{12} genome copies (gc)/ml;

AAV_8-CAG-FLEx^{FRT}-RABV-G, 1.3 × 10^{12} gc/mL;

AAV_{DJ}-hSyn-FLEx^{FRT}-hM4Di, 2.9 × 10^{13} gc/mL;

AAV_{DJ}-hSyn-FLEx^{FRT}-hM3Dq, 4.6 × 10^{13} gc/mL;

AAV_{DJ}-Ef1 α-fDio-EYFP, 3 × 10^{12} gc/mL;

AAV_5-EF1 α-fDIO-GCaMP6f, 7.3 × 10^{12} gc/mL;

AAV_{retro}-EF1 α-fDIO-Cre, 1.9 × 10^{13} gc/mL;

AAV_1hSyn-FLEx^{loxP}-jGCaMP7f, 1.2 × 10^{13} gc/mL;

AAV_{DJ}-hSyn-FLEx^{FRT}-mGFP-2A-Synaptophysin-mRuby, 3.7 × 10^{12} gc/mL;

CAV-FLEx^{loxP}-Flp, 5.0 × 10^{12} gc/mL;

RABVΔG, 5.0 × 10^8 cfu/mL.

Drug administration—Cocaine was administered (Intraperitoneal injections) at a dose of 15 mg/kg, morphine at 10 mg/kg, and CNO at 5 mg/kg.

Transsynaptic tracing/cTRIO—cTRIO experiments were performed as previously described (Beier et al., 2015), except that a single injection of cocaine (15 mg/kg) or saline was administered one day prior to RABV injection (Beier et al., 2017). We injected 500 nL of *CAV-FLEx^{loxP}-Flp* unilaterally into the amygdala, and during the same surgery, also injected 500 nL of a 1:1 volume mix of *AAV$_5$-FLEx^{FRT}-TC* and *AAV$_8$-FLEx^{FRT}-RABV-G* into the VTA. After 13 days, a single injection of cocaine or saline was given IP. A G-deleted, GFP-expressing, EnvA-pseudotyped RABV was injected into the VTA the following day. Animals were sacrificed five days following RABV injection.

In order to identify input changes that occur following an aversive foot shock, in a separate cohort of animals, 13 days following CAV/AAV injection animals were placed into an auditory fear conditioning chamber, as described in the behavior section below. RABV was injected 1 day later, and animals sacrificed five days subsequent, as described above.

Fluorescent *in situ* hybridization (FISH)—FISH was performed as descried by Kishi and colleagues (Kishi et al., 2019) with modifications. A programmable single-stranded synthesis method called the primer-exchange reaction (PER) was used to amplify the signal.

Probe selection—Sequences for 32 *Slc32a1* (vGAT) and 32 *Slc17a6* (vGluT2) probes (39 - 45 bp) covering the whole messenger RNAs were selected from the mm10 reference genome in oligoMiner (https://yin.hms.harvard.edu/oligoMiner/list.html). A 9 bp sequence (tttCATCATCAT) was added onto the 3' end of all probes as a short DNA primer for PER to generate repetitive PER concatemers. A 42 bp hairpin sequence (ACATCATCATGGGCCTTTTGGCCCATGATGATGTATGATGATG/3InvdT/) was used as a template for PER. As there is no G in the concatemers, the G-C pair in the hairpin template was used as a PER polymerase stopper in the absence of dGTP. A Clean G sequence (CCCCGAAAGTGGCCTCGGGCCTTTTGGCCCGAGGCCACTTTCG) was added to the reaction to deplete trace dGTP contamination. All probes and oligo sequences were ordered from IDT.

PER concatemerization—The 32 *Slc32a1* and *Slc17a6* probes were dissolved individually to get 100 μM stock solutions. The probe mixture was prepared by mixing the same volume of all 32 probe solutions. For a typical 100 μL reaction, the following components were included: 10 μL 10x PBS (final concentration for 1x PBS: 137 mM NaCl, 2.7 mM KCl, 10 mM Na_2HPO_4, 1.8 mM KH_2PO_4, pH 7.4), 10 μL MgSO4 (100 mM), 10 μL dNTPs (10 mM, mixture of dATP, dTTP, dCTP), 10 μL Clean G (2 μM), 10 μL hairpin template (10 μM), 6 μL BST LF polymerase (NEB M0275L), and 36 μL DEPC-treated H_2O. After the reaction was incubated at 37°C for 15 min to deplete all dGTP contamination, 8 μL probe mixture was added, and then the reaction was kept at 37°C for 3 hours to generate concatemers with an approximate size of 400-500 bp. The polymerase was inactivated by heating at 80°C for 20 min. A small amount (5 μL) of reaction was loaded into an agarose gel for electrophoresis to check the size of the probe.

Brain section preparation—Five days after cTRIO experiments were performed using the amygdala as an output site, mice were transcardially perfused with 1x PBS and then 4% formaldehyde in 1x PBS. Brains were removed and post-fixed in 4% formaldehyde for 24 hours, and then dehydrated with 30% sucrose. For long-term storage, brains were frozen in an ethanol and dry ice bath and then kept at −80°C. Immediately prior to performing *in situ* hybridization reactions, brains were cut into 30 μm slices using a cryostat and stored in DEPC treated 1x PBS. The brain sections covering BNST (AP +0.26 to −0.34) were divided equally into two sets. One set was probed for *Slc32a1* and the other for *Slc17a6*.

In situ *hybridization*—All containers and buffers were either RNase free or treated with DEPC. In 48 wells, brain sections were washed with 1x PBS for 10 min, incubated in 0.1 M triethanolamine (TEA) for 10 min, and then pretreated with 0.25% acetic anhydride in 0.1 M TEA for 10 min. After being washed with 2x SSC for 5 min, brain sections were incubated at 43°C in an oven in wash buffer A (40% formamide, 2x SCC pH 7, 0.2% Tween-20) for 1 hour, and then incubated with pre-warmed probe/hyb solution [50 μL PER concatemer in 450 μL hyb solution (40% formamide, 2x SSC pH 7, 0.2% Tween-20, and 10% dextran sulfate)] at 43°C overnight (18-20 hours). On the second day, brain sections were washed 2 × 30 min in wash buffer A, 2 × 45 min in wash buffer B (25% formamide, 2x SCC pH 7, 0.2% Tween-20), and 2 × 15 min in 2x SSCTw (0.2% tween) at 43°C. Brain sections were then washed 3 × 5 min in PBSTw (0.2% tween in 1x PBS) at room temperature and then incubated in 1 μM oligo imager (/5Alex647N/tt ATGATGATGT ATGATGATGT/3InvdT/) in 1x PBS solution with 0.2% tween-20 and 10% dextran sulfate at 37°C for 2 hrs. After the incubation, brain sections were washed 4 × 5 min in PBSTw at room temperature, and then mounted on Superfrost Plus Micro slides (VWR, cat# 48311-703). Once the brain sections were dry on the slide, slides were incubated in PBSTw with DAPI for 30 min, washed 3 × 5 min with PBSTw, and then Fluoromount-G™ (Invitrogen, cat# 00-4958-02) was applied. Slides were then covered with cover glass (Thermo Scientific, cat# 152460).

Imaging and cell counting—Confocal microscopy was performed using an inverted Zeiss LSM700 AxioObserver with a 20× air objective (Plan-Apochromat 20×/0.8). Laser lines used were 488 nm and 639 nm. Images were z stacks with 20 μm thickness in 2 μm steps. Fiji was used for cell counting. All observed GFP+ neurons in the BNST were quantified as either positive or negative for overlap with *Slc32a1* or *Slc17a6* (639 nm) probes.

Immunohistochemistry—The primary antibody chicken anti-GFP (Aves Labs) was used at 1:1,000, rabbit anti-TH (Millipore) at 1:1,000, and rat anti-mCherry (ThermoFisher) at 1:2,000. All secondary antibodies (Donkey anti-chicken AlexaFluor488, donkey anti-rat AlexaFluor 555, donkey anti-rabbit AlexaFluor 647) were used at a concentration of 1:250.

Axonal arborization mapping from BNST^{GABA} cells—Axonal tracing experiments were performed as previously described (Beier et al., 2015). We injected 500 nL of *AAV_{DJ}-hSyn-FLEx^{FRT}-mGFP-2A-Synaptophysin-mRuby* unilaterally into the BNST. After 2 months, animals were sacrificed, brains were cut with a thickness of 60 μm and

immunolabeled for GFP to enhance signal. Sections were imaged on an Olympus IX83 microscope using a 4x objective. Five brains were quantified.

Quantifications of puncta from $BNST^{GABA}$ neurons in the midbrain was performed as previously described (Beier et al., 2017). Briefly, animals were injected with saline or cocaine 24 hours prior to being sacrificed. Floating sections (60 μm) were stained using anti-mCherry and anti-GFP antibodies. Sections were imaged on a Zeiss 700 confocal microscope using a 63x objective, with image stacks containing 30 sections at 0.27 μm intervals using 2x averaging. Three images were taken of puncta in the SNr and PVT of each brain. Images were analyzed using Imaris (Bitplane). The surface function was used to obtain the volume of mGFP+ neurites and mRuby+ puncta, while the spots function was used to estimate the number of mRuby+ puncta. Data from the three slices from the SNr and PVT were averaged for each brain. Measurements from the SNr were normalized to those from the PVT.

Fiber photometry—Fiber photometry experiments were performed as previously described (Beier et al., 2017). To measure activity in $BNST^{GABA}$ cells, 500 nL of *AAV_5-EF1 α-fDIO-GCaMP6f* was injected into the BNST. A 400 μm diameter, 0.39NA optical fiber (THORLABS) was implanted at the same location. For $BNST^{GABA}$→midbrain neurons, 500 nL of *AAV_{retro}-EF1 α-fDIO-Cre* was injected into the ventral midbrain, 500 nL of *AAV_1-hSyn-FLEx^{loxP}-jCaMP7f* was injected in the BNST, and fibers implanted over the BNST. For VTA^{DA}→amygdala neurons, *AAV_5-EF1 α-fDIO-GCaMP6f* was injected into the VTA, 500 nL of *CAV-FLEx^{loxP}-Flp* was injected into the amygdala, and fibers were implanted over the VTA. Implants were placed approximately 0.3 mm above the site of viral injection and were secured to the skull with metal screws (Antrin Miniature Specialists), Metabond (Parkell), and Geristore dental epoxy (DenMat). Mice were allowed to recover for at least 4 weeks before experiments.

Fiber photometry recordings were made using previously described equipment (Lerner et al., 2015). Mice were run through an injection/behavior timeline shown in Figure 5A. In brief, 465 nm and 405 nm excitation light were controlled via a RZ5P real-time processor (Tucker Davis Technologies) using Synapse software, and were used to stimulate Ca^{2+}-dependent and isosbestic emission, respectively. All optical signals were band pass filtered with a Fluorescence Mini Cube FMC4 (Doric) and were measured with a femtowatt photoreceiver (2151; Newport). Signal processing was performed with MATLAB (MathWorks Inc.). Signals were first motion corrected by subtracting the least squares best fit of the control trace to the calcium signal. Data points containing large motion artifacts were then manually removed. To assess neural activity, we quantified the time spent above threshold, which was set at 2.91 times the median absolute deviation (MAD) of each day's recording, a value that equates to the 95% confidence interval for Gaussian data (Gunaydin et al., 2014).

Peri-stimulus time histograms (PSTHs)—PSTHs were generated using timestamps corresponding to certain behavioral events. Mouse behavior was recorded using Biobserve, which returns a frame-by-frame record of coordinates corresponding to the nose, center of body, and the base of the mouse's tail. After defining the borders of each behavior arena within Biobserve, a custom Python script was used to generate a list of timestamps

corresponding to selected behavioral events. These events are as follows: for both the CPP pre-test and post-test, the moment the mouse enters either the saline-paired or cocaine-paired chamber; for locomotion, the moment the mouse initiated or ceased movement; for OFT, the moment the mouse either entered or left the center zone (where the center zone is defined by a square 1/3 the area of the total arena); for EPM, the moment the mouse entered either the open or closed arms of the maze. The coordinate corresponding to the mouse's body center was used for all calculations. For locomotion, motion was calculated by taking the distance the center body coordinate moved from frame to frame. Because of some inherent variability in Biobserve's estimation of the center coordinate (even when the mouse was not moving), velocity below 1.25 cm/s was used as the threshold for no movement. A second MATLAB script aligned each behavioral timestamp with the raw photometry trace and resampled the Biobserve coordinates to match the sampling rate of the fiber photometry data. The PSTH curve was then generated by charting the mean Z-score during the three-second pre- and post-event time intervals centered around each behavioral event.

For constructing correlograms, Pearson's correlation was used to measure synchronization of PSTH curves per region pair for each test and measurement during the time interval of 0.5 seconds preceding and 1.5 seconds following each event. r^2 and p-values were visualized in heatmaps.

Behavioral assays

CPP—To test for drug-induced CPP, animals were first tested in a single drug pairing, two-chamber CPP test. Each chamber was given different wall contexts. On the first day, animals were initially placed into the right chamber, and allowed to freely explore both chambers for thirty minutes (pre-test). On the second day, animals were saline-conditioned to the left side, and on the following day, cocaine (or morphine)-conditioned to the right side. Drug conditioning was counterbalanced across the mice. On the fourth day, animals were again initially placed into the right chamber, and allowed to explore freely (post-test). In tests where hM4Di was used along with YFP-expressing controls, 5 mg/kg CNO was injected thirty minutes before the beginning of both the cocaine and saline pairings. In tests where hM3Dq and YFP controls were used, animals were also injected thirty minutes before being placed in the chamber, and no cocaine was given. CPP scores were computed as the subtracted CPP score, which equals time spent in the drug paired chamber [(posttest-pretest)/posttest]. Each session was 30 minutes.

Sensitization—To test sensitization, animals were habituated to open field boxes equipped with motion tracking for two days (receiving saline injections before each session). Boxes contained polka dotted contexts on the walls for the duration of the sensitization testing. Animals were then injected with cocaine (or morphine) immediately before entry into the open-field boxes, for five consecutive days, for 30 minutes each.

OFT/EPM—After waiting ten days following the final drug injection, we then tested the animals in the open field test and elevated plus maze for anxiety behaviors. For the OFT the time spent in the center square (1/3 of the total area of the arena) during a five-minute test period was calculated. The following day, animals were tested in the EPM. Animals were

placed at the end of one of the open arms, facing outwards, at the beginning of the trial. The percentage of time spent in the two open arms during the five-minute testing period was quantified. OFT experiments were performed at an illuminance level ~1000 lux, and EPM ~25 lux.

For fiber photometry experiments, behavioral assays were performed exactly as described above. For chemogenetic inhibition experiments to test the necessity of defined cell populations in behavioral adaptation, to inhibit projection-defined subsets of midbrain DA cells (Figures 1, S1 and S2), we used a viral-genetic intersectional method. We injected 500 nL of *CAV-FLEx^{loxP}-Flp* bilaterally into the NAcMed, NAcLat, DLS, or amygdala, or 2 μL into the mPFC to target DA neurons projecting to each of these sites. During the same surgery, 500 nL of *AAV$_{DJ}$-hSyn-FLEx^{FRT}-hM4Di* (or YFP) was injected bilaterally into the ventral midbrain. Animals were allowed 2 weeks to recover. 5 mg/kg CNO was injected IP 30 min before each injection of 15 mg/kg cocaine (or saline during CPP pairing and day 3 of locomotor habituation to test for CNO effects on basal locomotor activity).

For inhibition of BNST^{GABA} inputs to the midbrain and VTA^{DA}→amygdala collaterals in the BNST (Figure 4), hM4Di or YFP were expressed in either BNST^{GABA} or VTA^{DA}→amygdala cells, respectively. To inhibit activity in a target-specific fashion, we used CNO microspheres, as reported previously (Beier et al., 2017). CNO microspheres were synthesized to enable slow release of CNO after a single infusion. Degradex PLGA CNO microspheres were custom ordered from Phosphorex. Beads of target mean diameter 1 μm were dissolved in 0.5% trehalose at a concentration of 5 mg microsphere per ml. The estimated CNO loading efficiency was 5%, the estimated burst release was 50%, and the estimated release time was 7 days. The target concentration of CNO release at a steady state was 100 pg/h (Park et al., 2014; Stachniak et al., 2014).

Given the estimated release time of 7 days, we performed experiments under a condensed timeline to test CPP and sensitization while giving all cocaine doses within a 7-day period. Briefly, animals were habituated to the open field boxes for 2 days before starting CPP experiments. Animals then underwent their CPP pretests. On the following day, 500 nL of CNO microspheres were bilaterally injected into the midbrain or BNST. After allowing an additional day for recovery, animals were saline paired with one chamber, followed by a cocaine pairing with the opposite chamber on the same day. The following day, animals were first tested for CPP in the CPP boxes, then were administered cocaine in the open field boxes to start sensitization on the same day. Animals then received 1 dose of cocaine and their locomotion was quantified in the open field for the following four days. Animals then underwent ten days of forced abstinence followed by testing in the OFT and EPM. If significant effects were observed through chemogenetic perturbation of inputs from the targeted cells, we then performed CPP experiments starting with a pretest on day 1, saline and cocaine pairing on day 2, followed by a posttest on day 3, allowing us to perform the CPP over 3 days, as before. This was followed by the first day of sensitization experiments in the open field chamber the same day as the CPP posttest was conducted in order to mirror the first round of experimentation. The rest of the protocol was repeated verbatim.

For chemogenetic activation experiments, mice expressing hM3Dq or YFP in $VTA^{DA}\rightarrow$amygdala cells were injected with CNO 30 min before testing in the EPM or OFT.

Morphine CPP, sensitization, and EPM/OFT behavioral assays (Figures 6A–6D) were conducted exactly as for cocaine. 10 mg/kg morphine doses were administered each time, preceded 30 min by 5 mg/kg CNO according to the same protocol as for cocaine.

Reinstatement—For cocaine CPP reinstatement experiments in Figures 7C and 7D, cocaine CPP following a single drug pairing was performed as described above. Following CPP testing, CPP was then extinguished by placing the animals in the same CPP chambers for 2 subsequent days with no drug pairings. After a further 2-day break, animals were injected with CNO, followed 30 min later with a half normal dose of cocaine (7.5 mg/kg), and placed into the CPP chamber, where the time spent in the drug-paired chamber was assessed. Rather than calculating a subtracted CPP score, we report the total time spent in the drug-paired chamber during each 30-min session. For chemogenetic reinstatement where hM3Dq or YFP were expressed in $VTA^{da}\rightarrow$Amygdala cells, CPP was established with a single cocaine pairing, and that CPP was extinguished as above. On the reinstatement day, 5 mg/kg CNO was administered to the animals, and the animals were immediately placed into the open CPP apparatus.

Predator odor stress—2,4,5 trimethylthiazoline (TMT; Sigma), a constituent of fox urine that is innately aversive to rodents, was used for the predator odor. Scent was prepared by mixing 200 μL of TMT into 150 g standard mouse bedding and then dividing the scented bedding into 5 10-cm plastic petri dishes sealed with lab tape and perforated to allow the scent to escape. This preparation exposes each animal to approximately 40 μL TMT. Each experimental animal (YFP and hM4Di) was exposed to TMT in a standard mouse cage (36cm L x 20cm W x 13 cm D) for 1 h per day at the same time each day, for 4 consecutive days. Separate control (YFP) mice were handled 2 min per day by the experimenter for each of the 4 days and placed into new cages for 1 h but were not exposed to the predator odor. On the day following the final odor exposure, experimental and control mice were removed from the vivarium at the same time as the odor exposure was performed in previous days and moved to a different room for the EPM test.

Auditory fear conditioning—Mice were first habituated to the auditory fear conditioning chambers. Mice were individually placed in the chamber (Coulbourn Instruments) located in the center of a sound attenuating cubicle. The conditioning chamber was cleaned with 10% ethanol to provide a background odor. A ventilation fan provided a background noise at ~55 dB. After a 2 min exploration period, three 2 kHz, 85 dB tones were played, for 30s each, with a 90s interval between them. Following these initial tones, three subsequent tones were pained with a 1s, 0.75 mA foot shock. The foot shocks co-terminated with the tone. The mice remained in the chamber for another 60s before being returned to the home cages. RABV injections were then performed the following day.

QUANTIFICATION AND STATISTICAL ANALYSIS

All statistics were calculated using GraphPad Prism 9 software. Statistical significance between direct comparisons was assessed by unpaired or paired t-tests. When multiple conditions were compared, one-or two-way ANOVAs were first performed, as appropriate, and if significant differences were identified, t-tests were then performed for each individual comparison. Multiple comparisons corrections were performed when multiple such t-tests were being performed, and significance was assessed using the Holm-Bonferroni method. In conditions where multiple comparisons were performed and the results were still considered significant, asterisks were presented corresponding to the original p values. Where the differences were not significant when considering multiple comparisons (e.g., Figure 1I), the raw, uncorrected p values are provided on the graph. Dot plots presented throughout the manuscript include a bar representing the mean value for each group. Error bars represent s.e.m. throughout. For all figures, ns $p > 0.05$, *$p \leq 0.05$, **$p \leq 0.01$, ***$p \leq 0.001$, ****$p \leq 0.0001$.

Supplementary Material

Refer to Web version on PubMed Central for supplementary material.

ACKNOWLEDGMENTS

We would like to acknowledge Boris Heifets for providing and assisting with implementation of custom MATLAB scripts for fiber photometry analysis, Yihan Wang for computational assistance, and Greg Corder and Steve Mahler for critical analyses. This work was supported by the NIH (R00 DA041445 and DP2 AG067666), Tobacco-Related Disease Research Program (T31KT1437 and T31P1426), American Parkinson Disease Association (APDA-5589562), Alzheimer's Association (AARG-NTF-20-685694), New Vision Research (CCAD2020-002), and Brain and Behavior Research Foundation (NARSAD 26845) (to K.T.B.); T31DT1729 (to M.H.); and T32 GM136624-01 and NSF GRFP DGE-1839285 (to P.D.).

REFERENCES

Armbruster BN, Li X, Pausch MH, Herlitze S, and Roth BL (2007). Evolving the lock to fit the key to create a family of G protein-coupled receptors potently activated by an inert ligand. Proc. Natl. Acad. Sci. USA 104, 5163–5168. 10.1073/pnas.0700293104. [PubMed: 17360345]

Aston-Jones G, and Harris GC (2004). Brain substrates for increased drug seeking during protracted withdrawal. Neuropharmacology 47, 167–179. 10.1016/j.neuropharm.2004.06.020. [PubMed: 15464135]

Beier KT, Steinberg EE, Deloach KE, Xie S, Miyamichi K, Schwarz L, Gao XJ, Kremer EJ, Malenka RC, and Luo L (2015). Circuit architecture of VTA dopamine neurons revealed by systematic input-output mapping. Cell 162, 622–634. 10.1016/j.cell.2015.07.015. [PubMed: 26232228]

Beier KT, Kim CK, Hoerbelt P, Hung LW, Heifets BD, Deloach KE, Mosca TJ, Neuner S, Deisseroth K, Luo L, and Malenka RC (2017). Rabies screen reveals GPe control of cocaine-triggered plasticity. Nature 549, 345–350. 10.1038/nature23888. [PubMed: 28902833]

Beier KT, Gao XJ, Xie S, DeLoach KE, Malenka RC, and Luo L (2019). Topological organization of ventral tegmental area connectivity revealed by viral-genetic dissection of input-output relations. Cell Rep. 26, 159–167.e6. 10.1016/j.celrep.2018.12.040. [PubMed: 30605672]

Bromberg-Martin ES, Matsumoto M, and Hikosaka O (2010). Dopamine in motivational control: rewarding, aversive, and alerting. Neuron 68, 815–834. 10.1016/j.neuron.2010.11.022. [PubMed: 21144997]

Cahill L, and McGaugh JL (1990). Amygdaloid complex lesions differentially affect retention of tasks using appetitive and aversive reinforcement. Behav. Neurosci 104, 532–543. 10.1037/0735-7044.104.4.532. [PubMed: 2206424]

Di Chiara G, Bassareo V, Fenu S, De Luca MA, Spina L, Cadoni C, Acquas E, Carboni E, Valentini V, and Lecca D (2004). Dopamine and drug addiction: the nucleus accumbens shell connection. Neuropharmacology 47, 227–241. 10.1016/j.neuropharm.2004.06.032. [PubMed: 15464140]

Coque L, Mukherjee S, Cao JL, Spencer S, Marvin M, Falcon E, Sidor MM, Birnbaum SG, Graham A, Neve RL, et al. (2011). Specific role of VTA dopamine neuronal firing rates and morphology in the reversal of anxiety-related, but not depression-related behavior in the clockδ19 mouse model of mania. Neuropsychopharmacology 36, 1478–1488. 10.1038/npp.2011.33. [PubMed: 21430648]

de Oliveira AR, Reimer AE, de Macedo CEA, Carvalho MC, de Silva M.A. de S., and Brandão ML (2011). Conditioned fear is modulated by D2 receptor pathway connecting the ventral tegmental area and basolateral amygdala. Neurobiol. Learn. Mem 95, 37–45. 10.1016/j.nlm.2010.10.005. [PubMed: 20955808]

Debacker J, Hawken ER, Normandeau CP, Jones AA, Di Prospero C, Mechefske E, Gardner Gregory J, Hayton SJ, and Dumont ÉC (2015). GluN2B-containing NMDA receptors blockade rescues bidirectional synaptic plasticity in the bed nucleus of the stria terminalis of cocaine self-administering rats. Neuropsychopharmacology 40, 394–405. 10.1038/npp.2014.182. [PubMed: 25035084]

Deckers L (2016). Addictions and addictive behaviors. In Motivation: Biological, Psychological, and Environmental (Routledge).

Delfs JM, Zhu Y, Druhan JP, and Aston-Jones G (2000). Noradrenaline in the ventral forebrain is critical for opiate withdrawal-induced aversion. Nature 403, 430–434. 10.1038/35000212. [PubMed: 10667795]

Dole VP, Nyswander ME, and Kreek MJ (1966). Narcotic blockade. Arch. Intern. Med 118, 304–309. 10.1001/archinte.1966.00290160004002. [PubMed: 4162686]

Dong HW, and Swanson LW (2004). Projections from bed nuclei of the stria terminalis, posterior division: implications for cerebral hemisphere regulation of defensive and reproductive behaviors. J. Comp. Neurol 471, 396–433. 10.1002/cne.20002. [PubMed: 15022261]

Dong HW, and Swanson LW (2006a). Projections from bed nuclei of the stria terminalis, anteromedial area: cerebral hemisphere integration of neuroendocrine, autonomic, and behavioral aspects of energy balance. J. Comp. Neurol 494, 142–178. 10.1002/cne.20788. [PubMed: 16304685]

Dong HW, and Swanson LW (2006b). Projections from bed nuclei of the stria terminalis, dorsomedial nucleus: implications for cerebral hemisphere integration of neuroendocrine, autonomic, and drinking responses. J. Comp. Neurol 494, 75–107. 10.1002/cne.20790. [PubMed: 16304681]

Dong Y, Saal D, Thomas M, Faust R, Bonci A, Robinson T, and Malenka RC (2004). Cocaine-induced potentiation of synaptic strength in dopamine neurons: behavioral correlates in GluRA(−/−) mice. Proc. Natl. Acad. Sci. USA 101, 14282–14287. 10.1073/pnas.0401553101. [PubMed: 15375209]

Dumont EC, Mark GP, Mader S, and Williams JT (2005). Self-administration enhances excitatory synaptic transmission in the bed nucleus of the stria terminalis. Nat. Neurosci 8, 413–414. 10.1038/nn1414. [PubMed: 15735642]

Dumont ÉC, Rycroft BK, Maiz J, and Williams JT (2008). Morphine produces circuit-specific neuroplasticity in the bed nucleus of the stria terminalis. Neuroscience 153, 232–239. 10.1016/j.neuroscience.2008.01.039. [PubMed: 18343592]

Everitt BJ, Cardinal RN, Hall J, Parkinson JA, and Robbins TW (2000). Differential involvement of amygdala subsystems in appetitive conditioning and drug addiction. In The Amygdala: A Functional Analysis(Oxford University Press), pp. 353–390.

Francesconi W, Szücs A, Berton F, Koob GF, Vendruscolo LF, and Sanna PP (2017). Opiate dependence induces cell type-specific plasticity of intrinsic membrane properties in the rat juxtacapsular bed nucleus of stria terminalis (jcBNST). Psychopharmacology (Berl) 234, 3485–3498. 10.1007/s00213-017-4732-4. [PubMed: 28986608]

Gallagher M (2000). The amygdala and associative learning. In The Amygdala: A Functional Analysis (Oxford University Press), pp. 311–329.

Georges F, and Aston-Jones G (2001). Potent regulation of midbrain dopamine neurons by the bed nucleus of the stria terminalis. J. Neurosci 21, RC160. 10.1523/jneurosci.21-16-j0003.2001. [PubMed: 11473131]

Georges F, and Aston-Jones G (2002). Activation of ventral tegmental area cells by the bed nucleus of the stria terminalis: a novel excitatory amino acid input to midbrain dopamine neurons. J. Neurosci 22, 5173–5187. 10.1523/jneurosci.22-12-05173.2002. [PubMed: 12077212]

Gunaydin LA, Grosenick L, Finkelstein JC, Kauvar IV, Fenno LE, Adhikari A, Lammel S, Mirzabekov JJ, Airan RD, Zalocusky KA, et al. (2014). Natural neural projection dynamics underlying social behavior. Cell 157, 1535–1551. 10.1016/j.cell.2014.05.017. [PubMed: 24949967]

Jalabert M, Aston-Jones G, Herzog E, Manzoni O, and Georges F (2009). Role of the bed nucleus of the stria terminalis in the control of ventral tegmental area dopamine neurons. Prog. Neuropsychopharmacol. Biol. Psychiatry 33, 1336–1346. 10.1016/j.pnpbp.2009.07.010. [PubMed: 19616054]

Jennings JH, Sparta DR, Stamatakis AM, Ung RL, Pleil KE, Kash TL, and Stuber GD (2013). Distinct extended amygdala circuits for divergent motivational states. Nature 496, 224–228. 10.1038/nature12041. [PubMed: 23515155]

Kash TL, Nobis WP, Matthews RT, and Winder DG (2008). Dopamine enhances fast excitatory synaptic transmission in the extended amygdala by a CRF-R1-dependent process. J. Neurosci 28, 13856–13865. 10.1523/jneurosci.4715-08.2008. [PubMed: 19091975]

Kash TL, Pleil KE, Marcinkiewcz CA, Lowery-Gionta EG, Crowley N, Mazzone C, Sugam J, Andrew Hardaway J, and McElligott ZA (2015). Neuropeptide regulation of signaling and behavior in the BNST. Mol. Cells 38, 1–13. 10.14348/molcells.2015.2261. [PubMed: 25475545]

Kim S-Y, Adhikari A, Lee SY, Marshel JH, Kim CK, Mallory CS, Lo M, Pak S, Mattis J, Lim BK, et al. (2013). Diverging neural pathways assemble a behavioural state from separable features in anxiety. Nature 496, 219–223. 10.1038/nature12018. [PubMed: 23515158]

Kishi JY, Lapan SW, Beliveau BJ, West ER, Zhu A, Sasaki HM, Saka SK, Wang Y, Cepko CL, and Yin P (2019). SABER amplifies FISH: enhanced multiplexed imaging of RNA and DNA in cells and tissues. Nat. Methods 16, 533–544. 10.1038/s41592-019-0404-0. [PubMed: 31110282]

Koob GF (2009). Neurobiological substrates for the dark side of compulsivity in addiction. Neuropharmacology 56, 18–31. 10.1016/j.neuropharm.2008.07.043. [PubMed: 18725236]

Koob GF, and Le Moal M (1997). Drug abuse: hedonic homeostatic dysregulation. Science 278, 52–58. 10.1126/science.278.5335.52. [PubMed: 9311926]

Koob GF, and Le Moal M (2001). Drug addiction, dysregulation of reward, and allostasis. Neuropsychopharmacology 24, 97–129. 10.1016/s0893-133x(00)00195-0. [PubMed: 11120394]

Koob GF, Ahmed SH, Boutrel B, Chen SA, Kenny PJ, Markou A, O'Dell LE, Parsons LH, and Sanna PP (2004). Neurobiological mechanisms in the transition from drug use to drug dependence. Neurosci. Biobehav. Rev 27, 739–749. 10.1016/j.neubiorev.2003.11.007. [PubMed: 15019424]

Kudo T, Uchigashima M, Miyazaki T, Konno K, Yamasaki M, Yanagawa Y, Minami M, and Watanabe M (2012). Three types of neurochemical projection from the bed nucleus of the stria terminalis to the ventral tegmental area in adult mice. J. Neurosci 32, 18035–18046. 10.1523/jneuro-sci.4057-12.2012. [PubMed: 23238719]

Lammel S, Ion DI, Roeper J, and Malenka RC (2011). Projection-specific modulation of dopamine neuron synapses by aversive and rewarding stimuli. Neuron 70, 855–862. 10.1016/j.neuron.2011.03.025. [PubMed: 21658580]

Lammel S, Lim BK, Ran C, Huang KW, Betley MJ, Tye KM, Deisseroth K, and Malenka RC (2012). Input-specific control of reward and aversion in the ventral tegmental area. Nature 491, 212–217. 10.1038/nature11527. [PubMed: 23064228]

Lammel S, Lim BK, and Malenka RC (2014). Reward and aversion in a heterogeneous midbrain dopamine system. Neuropharmacology 76, 351–359. 10.1016/j.neuropharm.2013.03.019. [PubMed: 23578393]

Ledoux JE (2000). Emotion circuits in the brain. Annu. Rev. Neurosci 23, 155–184. 10.1146/annurev.neuro.23.1.155. [PubMed: 10845062]

Lerner TN, Shilyansky C, Davidson TJ, Evans KE, Beier KT, Zalocusky KA, Crow AK, Malenka RC, Luo L, Tomer R, and Deisseroth K (2015). Intact-brain analyses reveal distinct information carried by SNc dopamine subcircuits. Cell 162, 635–647. 10.1016/j.cell.2015.07.014. [PubMed: 26232229]

Lin R, Liang J, Wang R, Yan T, Zhou Y, Liu Y, Feng Q, Sun F, Li Y, Li A, et al. (2020). The raphe dopamine system controls the expression of incentive memory. Neuron 106, 498–514.e8. 10.1016/j.neuron.2020.02.009. [PubMed: 32145184]

Lüscher C, and Malenka RC (2011). Drug-evoked synaptic plasticity in addiction: from molecular changes to circuit remodeling. Neuron 69, 650–663. 10.1016/j.neuron.2011.01.017. [PubMed: 21338877]

Lutas A, Kucukdereli H, Alturkistani O, Carty C, Sugden AU, Fernando K, Diaz V, Flores-Maldonado V, and Andermann ML (2019). State-specific gating of salient cues by midbrain dopaminergic input to basal amygdala. Nat. Neurosci 22, 1820–1833. 10.1038/s41593-019-0506-0. [PubMed: 31611706]

Mameli M, Halbout B, Creton C, Engblom D, Parkitna JR, Spanagel R, and Lüscher C (2009). Cocaine-evoked synaptic plasticity: persistence in the VTA triggers adaptations in the NAc. Nat. Neurosci 12, 1036–1041. 10.1038/nn.2367. [PubMed: 19597494]

Martin WR, and Jasinski DR (1969). Physiological parameters of morphine dependence in man-Tolerance, early abstinence, protracted abstinence. J. Psychiatr. Res 7, 9–17. 10.1016/0022-3956(69)90007-7. [PubMed: 5352850]

McFarland K, Davidge SB, Lapish CC, and Kalivas PW (2004). Limbic and motor circuitry underlying footshock-induced reinstatement of cocaine-seeking behavior. J. Neurosci 24, 1551–1560. 10.1523/jneuro-sci.4177-03.2004. [PubMed: 14973230]

Meil WM, and See RE (1997). Lesions of the basolateral amygdala abolish the ability of drug associated cues to reinstate responding during withdrawal from self-administered cocaine. Behav. Brain Res 87, 139–148. 10.1016/s0166-4328(96)02270-x. [PubMed: 9331482]

Menegas W, Akiti K, Amo R, Uchida N, and Watabe-Uchida M (2018). Dopamine neurons projecting to the posterior striatum reinforce avoidance of threatening stimuli. Nat. Neurosci 21, 1421–1430. 10.1038/s41593-018-0222-1. [PubMed: 30177795]

Nestler EJ (2005). Is there a common molecular pathway for addiction? Nat. Neurosci 8, 1445–1449. 10.1038/nn1578. [PubMed: 16251986]

Nguyen C, Mondoloni S, Le Borgne T, Centeno I, Come M, Jehl J, Solie C, Reynolds LM, Durang-de Cuttoli R, Tolu S, et al. (2021). Nicotine inhibits the VTA-to-amygdala dopamine pathway to promote anxiety. Neuron 109, 2604–2615.e9. 10.1016/j.neuron.2021.06.013. [PubMed: 34242565]

Olive MF, Koenig HN, Nannini MA, and Hodge CW (2002). Elevated extracellular CRF levels in the bed nucleus of the stria terminalis during ethanol withdrawal and reduction by subsequent ethanol intake. Pharmacol. Biochem. Behav 72, 213–220. 10.1016/s0091-3057(01)00748-1. [PubMed: 11900791]

de Oliveira AR, Reimer AE, and Brandão ML (2009). Role of dopamine receptors in the ventral tegmental area in conditioned fear. Behav. Brain Res 199, 271–277. 10.1016/j.bbr.2008.12.004. [PubMed: 19111792]

Park JS, Rhau B, Hermann A, McNally KA, Zhou C, Gong D, Weiner OD, Conklin BR, Onuffer J, and Lim WA (2014). Synthetic control of mammalian-cell motility by engineering chemotaxis to an orthogonal bioinert chemical signal. Proc. Natl. Acad. Sci. U S A 111, 5896–5901. 10.1073/pnas.1402087111. [PubMed: 24711398]

Pignatelli M, and Bonci A (2015). Role of dopamine neurons in reward and aversion: a synaptic plasticity perspective. Neuron 86, 1145–1157. 10.1016/j.neuron.2015.04.015. [PubMed: 26050034]

Robinson TE, and Berridge KC (2000). The psychology and neurobiology of addiction: an incentive-sensitization view. Addiction 95, 91–117. 10.1046/j.1360-0443.95.8s2.19.x.

Robinson TE, and Berridge KC (2001). Incentive-sensitization and addiction. Addiction 96, 103–114. 10.1046/j.1360-0443.2001.9611038.x. [PubMed: 11177523]

Robinson TE, and Berridge KC (2008). The incentive sensitization theory of addiction: some current issues. Philos. Trans. R. Soc. B Biol. Sci 363, 3137–3146. 10.1098/rstb.2008.0093.

Rosen JB, Asok A, and Chakraborty T (2015). The smell of fear: innate threat of 2,5-dihydro-2,4,5-trimethylthiazoline, a single molecule component of a predator odor. Front. Neurosci 9, 1–12. 10.3389/fnins.2015.00292. [PubMed: 25653585]

Sanchis-Segura C, and Spanagel R (2006). Behavioural assessment of drug reinforcement and addictive features in rodents: an overview. Addict. Biol 11, 2–38. 10.1111/j.1369-1600.2006.00012.x. [PubMed: 16759333]

Sartor GC, and Aston-Jones G (2012). Regulation of the ventral tegmental area by the bed nucleus of the stria terminalis is required for expression of cocaine preference. Eur. J. Neurosci 36, 3549–3558. 10.1111/j.1460-9568.2012.08277.x. [PubMed: 23039920]

Schultz W (2007). Multiple dopamine functions at different time courses. Annu. Rev. Neurosci 30, 259–288. 10.1146/annurev.neuro.28.061604.135722. [PubMed: 17600522]

Schwarz LA, Miyamichi K, Gao XJ, Beier KT, Weissbourd B, DeLoach KE, Ren J, Ibanes S, Malenka RC, Kremer EJ, and Luo L (2015). Viral-genetic tracing of the input–output organization of a central noradrenaline circuit. Nature 524, 88–92. 10.1038/nature14600. [PubMed: 26131933]

Shalev U, Morales M, Hope B, Yap J, and Shaham Y (2001). Time-dependent changes in extinction behavior and stress-induced reinstatement of drug seeking following withdrawal from heroin in rats. Psychopharmacology (Berl) 156, 98–107. 10.1007/s002130100748. [PubMed: 11465640]

Silberman Y, Matthews RT, and Winder DG (2013). A corticotropin releasing factor pathway for ethanol regulation of the ventral tegmental area in the bed nucleus of the stria terminalis. J. Neurosci 33, 950–960. 10.1523/jneurosci.2949-12.2013. [PubMed: 23325234]

Stachniak TJ, Ghosh A, and Sternson SM (2014). Chemogenetic synaptic silencing of neural circuits localizes a Hypothalamus→Midbrain pathway for feeding behavior. Neuron 82, 797–808. 10.1016/j.neuron.2014.04.008. [PubMed: 24768300]

Tang W, Kochubey O, Kintscher M, and Schneggenburger R (2020). A VTA to basal amygdala dopamine projection contributes to signal salient somatosensory events during fear learning. J. Neurosci 40, 3969–3980. 10.1523/jneurosci.1796-19.2020. [PubMed: 32277045]

Tervo DGR, Hwang BY, Viswanathan S, Gaj T, Lavzin M, Ritola KD, Lindo S, Michael S, Kuleshova E, Ojala D, et al. (2016). A designer AAV variant permits efficient retrograde Access to projection neurons. Neuron 92, 372–382. 10.1016/j.neuron.2016.09.021. [PubMed: 27720486]

Tian J, Huang R, Cohen JY, Osakada F, Kobak D, Machens CK, Callaway EM, Uchida N, and Watabe-Uchida M (2016). Distributed and mixed information in monosynaptic inputs to dopamine neurons. Neuron 91, 1374–1389. 10.1016/j.neuron.2016.08.018. [PubMed: 27618675]

Torres GE, Gainetdinov RR, and Caron MG (2003). Plasma membrane monoamine transporters: structure, regulation and function. Nat. Rev. Neurosci 4, 13–25. 10.1038/nrn1008. [PubMed: 12511858]

Tzschentke TM (2007). Measuring reward with the conditioned place preference (CPP) paradigm: update of the last decade. Addict. Biol 12, 227–462. 10.1111/j.1369-1600.2007.00070.x. [PubMed: 17678505]

Volkow ND, Fowler JS, Wang G-J, and Swanson JM (2004). Dopamine in drug abuse and addiction: results from imaging studies and treatment implications. Mol. Psychiatry 9, 557–569. 10.1038/sj.mp.4001507. [PubMed: 15098002]

Wise RA (2004). Dopamine, learning and motivation. Nat. Rev. Neurosci 5, 483–494. 10.1038/nrn1406. [PubMed: 15152198]

Highlights

- Unbiased RABV screen identifies drug-induced changes in rodent brain
- $BNST^{GABA}\rightarrow$midbrain cell activity is elevated after a single cocaine exposure
- $BNST^{GABA}\rightarrow VTA^{DA}\rightarrow$amygdala pathway controls cocaine-induced anxiety and reinstatement
- $VTA^{DA}\rightarrow$amygdala cells are necessary and sufficient to drive general anxiety states

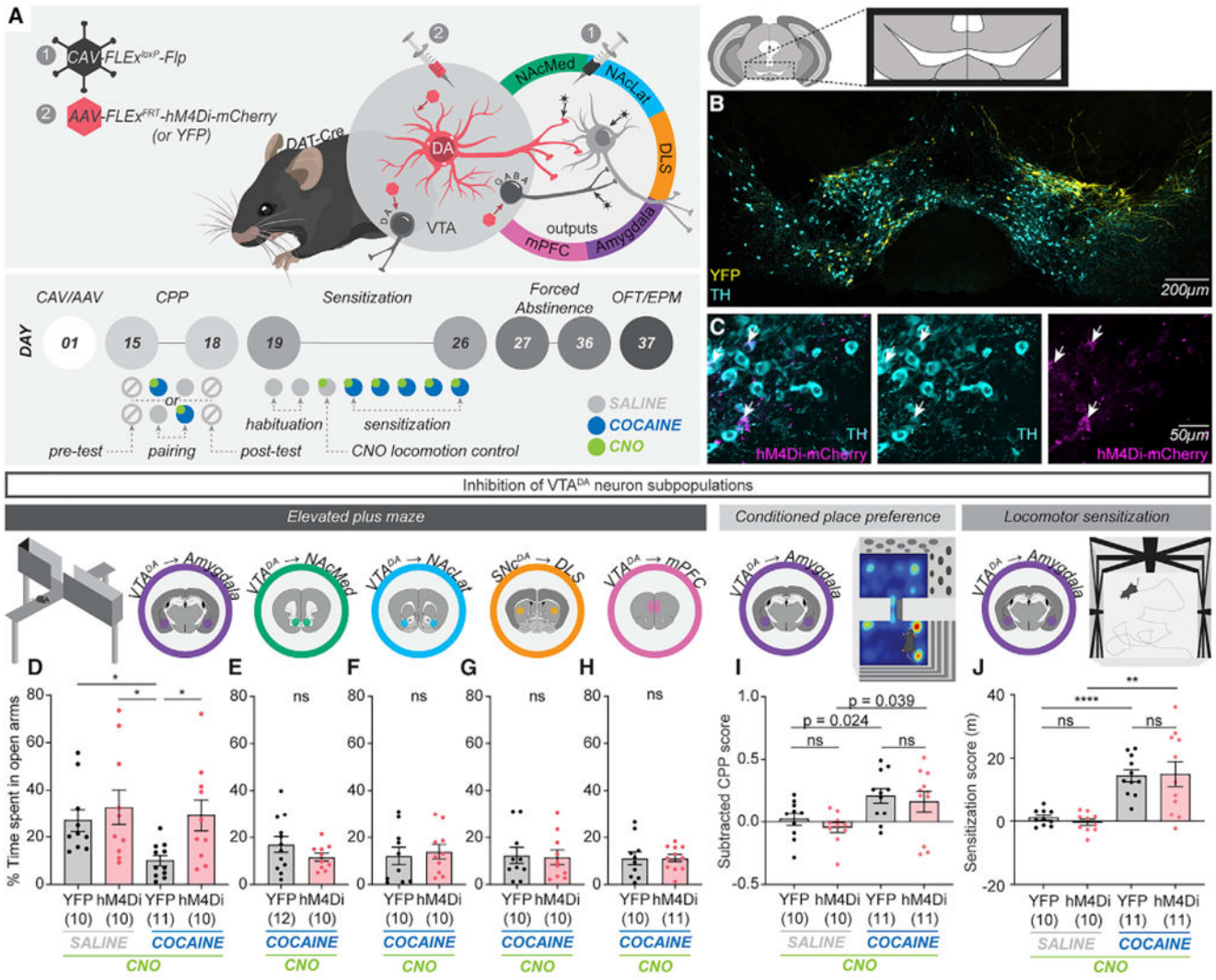

Figure 1. Activity in VTA^{DA}→amygdala cells is selectively required for cocaine-induced anxiety

(A) Schematic and timeline of the experiments. CPP, conditioned place preference; OFT, open field test; EPM, elevated plus maze.

(B) Expression of YFP in VTA^{DA}→amygdala cells.

(C) Overlap of Flp-dependent hM4Di expression with tyrosine hydroxylase.

(D) The reduction in the time spent in the open arms of the EPM during protracted withdrawal after repeated cocaine administration was blocked by hM4Di-mediated inhibition of VTA^{DA}→amygdala cells during cocaine administration (YFP saline versus YFP cocaine, p = 0.0032; YFP saline versus hM4Di saline, p = 0.53; YFP saline versus hM4Di cocaine, p = 0.79; YFP cocaine versus hM4Di saline, p = 0.0064; YFP cocaine versus hM4Di cocaine, p = 0.01; hM4Di saline versus hM4Di cocaine, p = 0.73; n = 10 YFP/saline, 10 hM4Di/saline, 11 YFP/cocaine, 10 hM4Di/cocaine).

(E–H) Inhibition of VTA^{DA}→NAcMed (p = 0.94, n = 12 YFP/cocaine, 10 hM4Di/cocaine), VTA^{DA}→NAcLat (p = 0.71, n = 10 YFP/cocaine, 10 hM4Di/cocaine), SNc^{DA}→DLS (p = 0.87, n = 10 YFP/cocaine, 10 hM4Di/cocaine), or VTA^{DA}→mPFC (p = 0.99, n = 10

YFP/cocaine, 11 hM4Di/cocaine) cells had no consequences for anxiety as assessed using the EPM.

(I and J) Inhibition of $VTA^{DA}\rightarrow$amygdala cells during cocaine administration had no effects on cocaine CPP (YFP saline versus YFP cocaine, $p = 0.024$; YFP saline versus hM4Di saline, $p = 0.31$; YFP saline versus hM4Di cocaine, $p = 0.16$; YFP cocaine versus hM4Di saline, $p = 0.0022$; YFP cocaine versus hM4Di cocaine, $p = 0.65$; hM4Di saline versus hM4Di cocaine, $p = 0.39$; n = 10 YFP/saline, 10 hM4Di/saline, 11 YFP/cocaine, 11 hM4Di/cocaine) (I) or locomotor sensitization (YFP saline versus YFP cocaine, $p < 0.0001$; YFP saline versus hM4Di saline, $p = 0.26$; YFP saline versus hM4Di cocaine, $p = 0.0035$; YFP cocaine versus hM4Di saline, $p < 0.0001$; YFP cocaine versus hM4Di cocaine, $p = 0.91$; hM4Di saline versus hM4Di cocaine, $p = 0.0017$; n = 10 YFP/saline, 10 hM4Di/saline, 11 YFP/cocaine, 11 hM4Di/cocaine) (J). Error bars in this figure and throughout the manuscript indicate ± 1 SEM. For all figures, ns $p > 0.05$, *$p \leq 0.05$, **$p \leq 0.01$, ***$p \leq 0.001$, ****$p \leq 0.0001$.

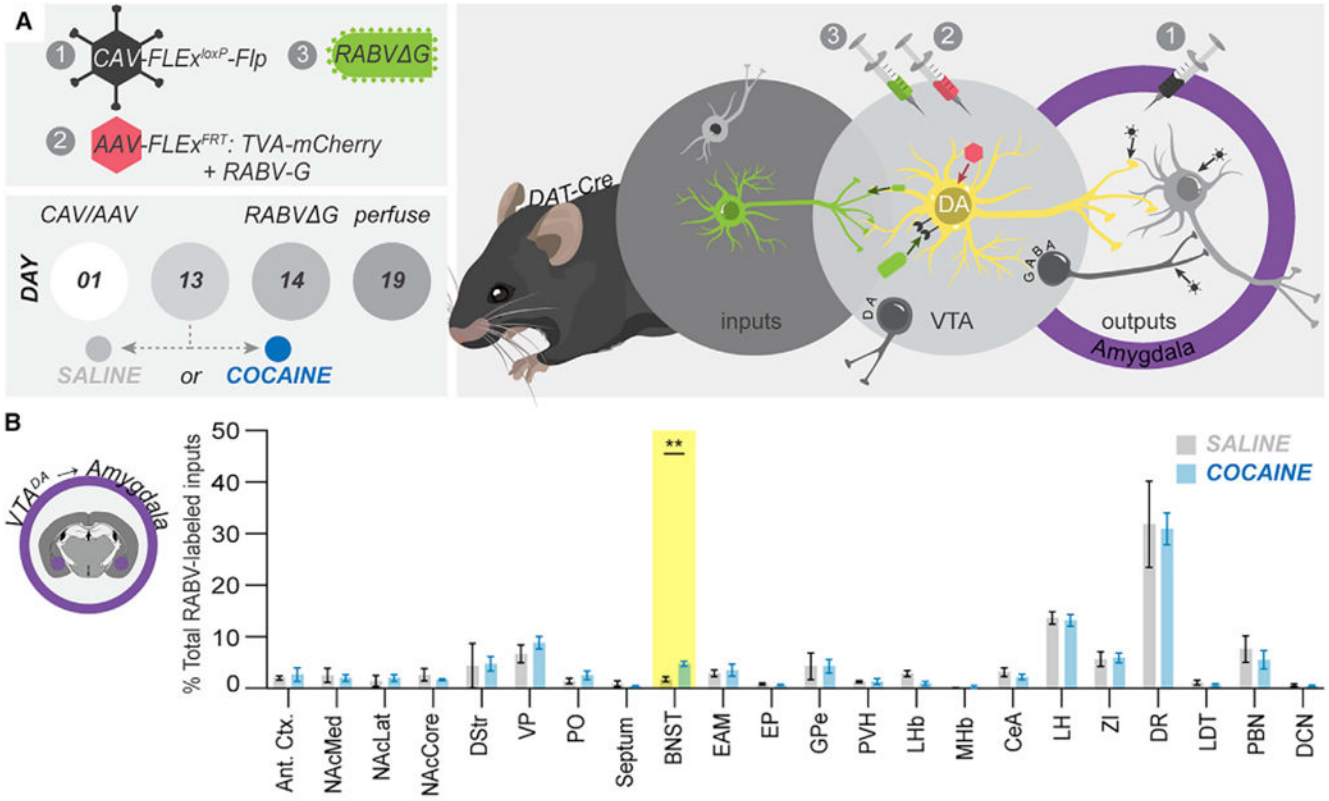

Figure 2. cTRIO detects an increase in BNST input labeling onto VTA^{DA}→amygdala cells in cocaine-treated mice.

(A) Schematic and timeline of cTRIO experiments.

(B) Cocaine triggered an increase in RABV-labeled inputs from the BNST onto VTA^{DA}→amygdala cells ($p = 0.0014$, $n = 4$ each).

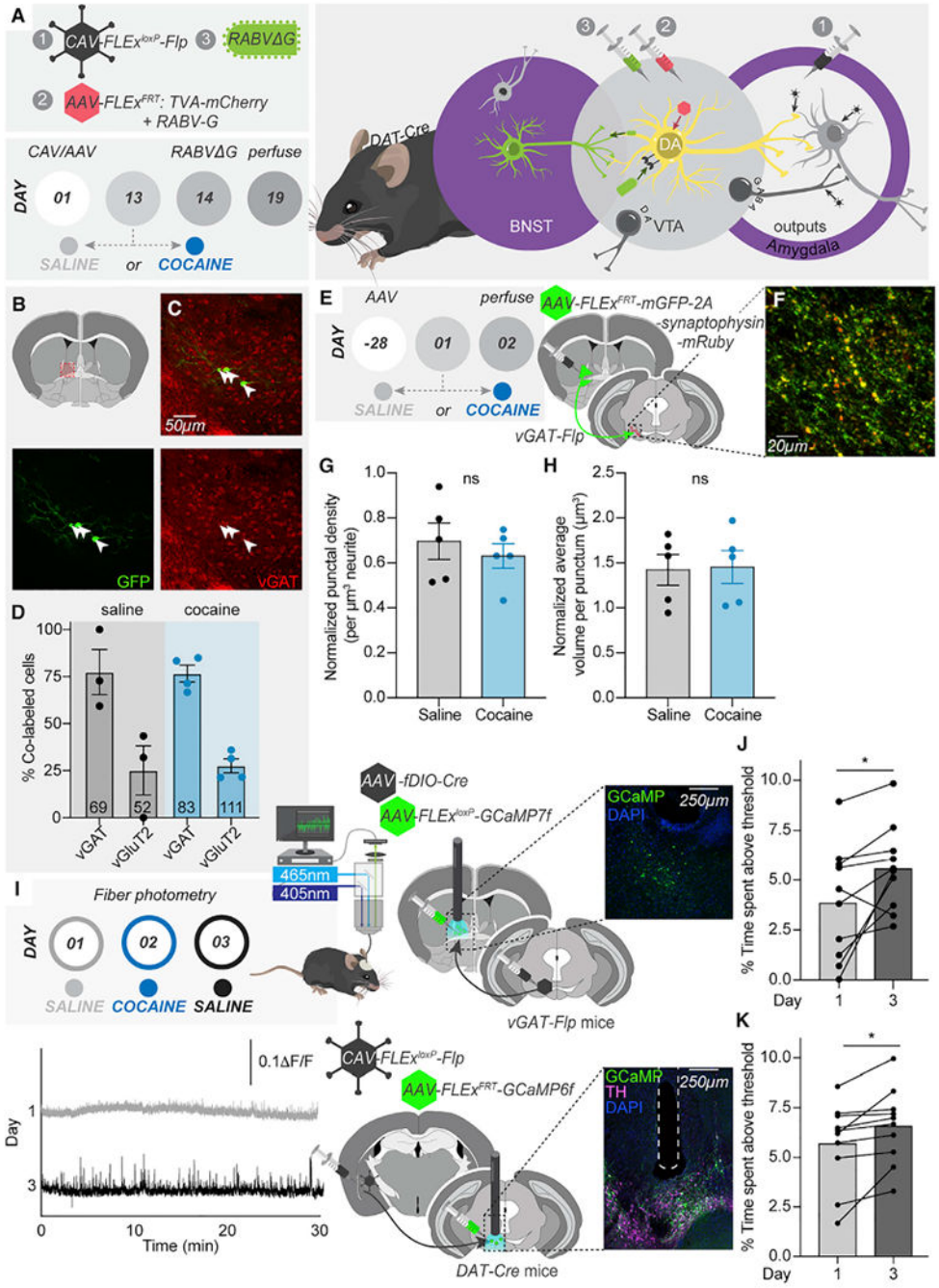

Figure 3. A single dose of cocaine causes long-lasting changes in the spontaneous activity of BNST^{GABA} and VTA^{DA}→amygdala cells.

(A) Schematic of cTRIO experiments to label BNST cells projecting to VTA^{DA}→amygdala cells.

(B) Fluorescence *in situ* hybridization (FISH) experiments were performed, focusing on the BNST.

(C) Probes to *Slc32a1* (vGAT) or *Slc17a6* (vGluT2) were used to identify GABAergic or glutamatergic neurons, respectively.

(D) Quantification of overlap of RABV-labeled cells with FISH probes. n = 3 saline, n = 4 cocaine.

(E) Timeline and schematic of putative synapse quantification.

(F) Sample image of GFP axons and synaptophysin-mRuby puncta in the ventral midbrain.

(G) No change in the density of puncta was observed (saline versus cocaine, p = 0.52, n = 5 each).

(H) No change in the volume of puncta was observed (saline versus cocaine, p = 0.90, n = 5 each).

(I) Schematic and timeline of fiber photometry experiments as well as representative traces from D1 and D3 in $BNST^{GABA}\rightarrow$midbrain cells.

(J) A single dose of cocaine caused a long-lasting increase in activity of $BNST^{GABA}\rightarrow$midbrain cells (D1 versus D3, p =0.018,n = 10).

(K) A single dose of cocaine caused a long-lasting increase in activity of $VTA^{DA}\rightarrow$amygdala cells (D1 versus D3, p = 0.01, n = 10).

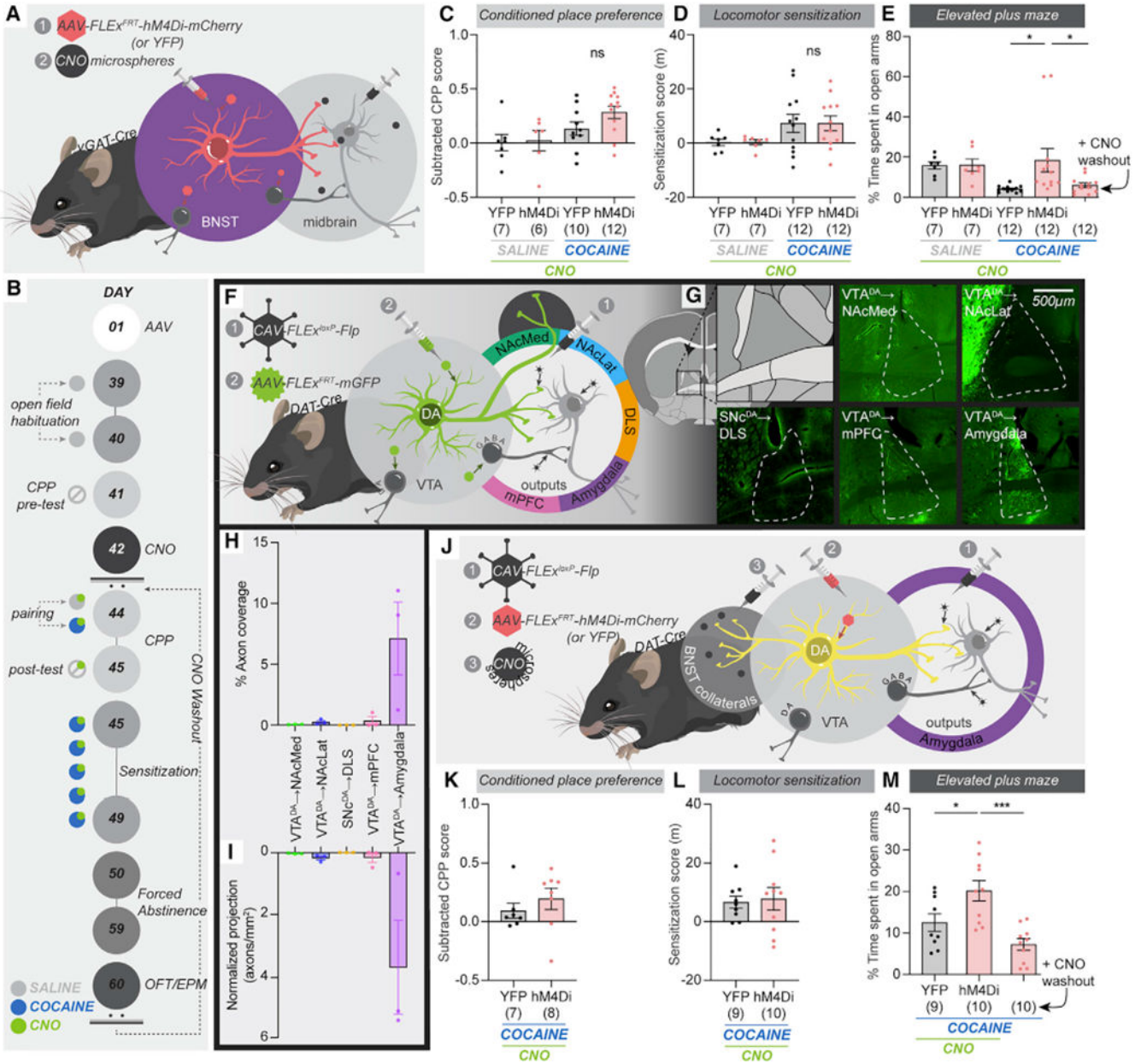

Figure 4. Inhibition of BNST^{GABA}→midbrain cells and collaterals from VTA^{DA}→amygdala cells in the BNST prevent development of cocaine withdrawal-induced anxiety.

(A) Strategy for terminal inhibition.

(B) Timeline for the experiments.

(C–E) Inhibition of BNST^{GABA}terminals in the midbrain had no effect on CPP (YFP saline versus YFP cocaine, p = 0.20; YFP saline versus hM4Di saline, p = 0.87; YFP saline versus hM4Di cocaine, p = 0.0069; YFP cocaine versus hM4Di saline, p = 0.30; YFP cocaine versus hM4Di cocaine, p = 0.095; hM4Di saline versus hM4Di cocaine, p = 0.015; n = 7 YFP/saline, 6 hM4Di/saline, 10 YFP/cocaine, and 12 hM4Di/cocaine)(C) or sensitization (YFP saline versus YFP cocaine, p = 0.17; YFP saline versus hM4Di saline, p = 0.67; YFP saline versus hM4Di cocaine, p = 0.17; YFP cocaine versus hM4Di saline, p = 0.089; YFP

cocaine versus hM4Di cocaine, p = 1.0; hM4Di saline versus hM4Di cocaine, p = 0.089; n = 7 YFP/saline, 7 hM4Di/saline, 12 YFP/cocaine, and 12 hM4Di/cocaine).

(D) but did prevent development of anxiety (YFP saline versus YFP cocaine, p = 0.0028; YFP saline versus hM4Di saline, p = 0.30; YFP saline versus hM4Di cocaine, p = 0.48; YFP cocaine versus hM4Di saline, p = 0.065; YFP cocaine versus hM4Di cocaine, p = 0.0089; hM4Di saline versus hM4Di cocaine, p = 0.65; hM4Di versus washout, p = 0.0094; n = 7 YFP/saline, 7 hM4Di/saline, 12 YFP/cocaine, 12 hM4Di/cocaine, and 12 hM4Di/cocaine washout) (E).

(F) Strategy for axon arbor quantification.

(G) Sample images of collaterals in the BNST from each of the five targeted midbrain DA cell populations.

(H) Percentage of the area in the BNST covered by axons from each midbrain DA cell population (n = 3 each).

(I) Projection density (axons per square millimeter) in the BNST from each midbrain DA cell population (n = 3 each).

(J) Strategy for collateral inhibition.

(K–M) Inhibition of terminals in the BNST from $VTA^{DA}\rightarrow$amygdala neurons during cocaine administration had no effect on CPP (YFP versus hM4Di, p = 0.39; n = 7 YFP, 8 hM4Di) (K) or sensitization (YFP versus hM4Di, p = 0.80; n = 9 YFP, 10 hM4Di) (L) but did prevent development of anxiety (YFP versus hM4Di, p = 0.032; hM4Di versus washout, p < 0.0001; n = 9 YFP, 10 hM4Di, 10 hM4Di washout) (M).

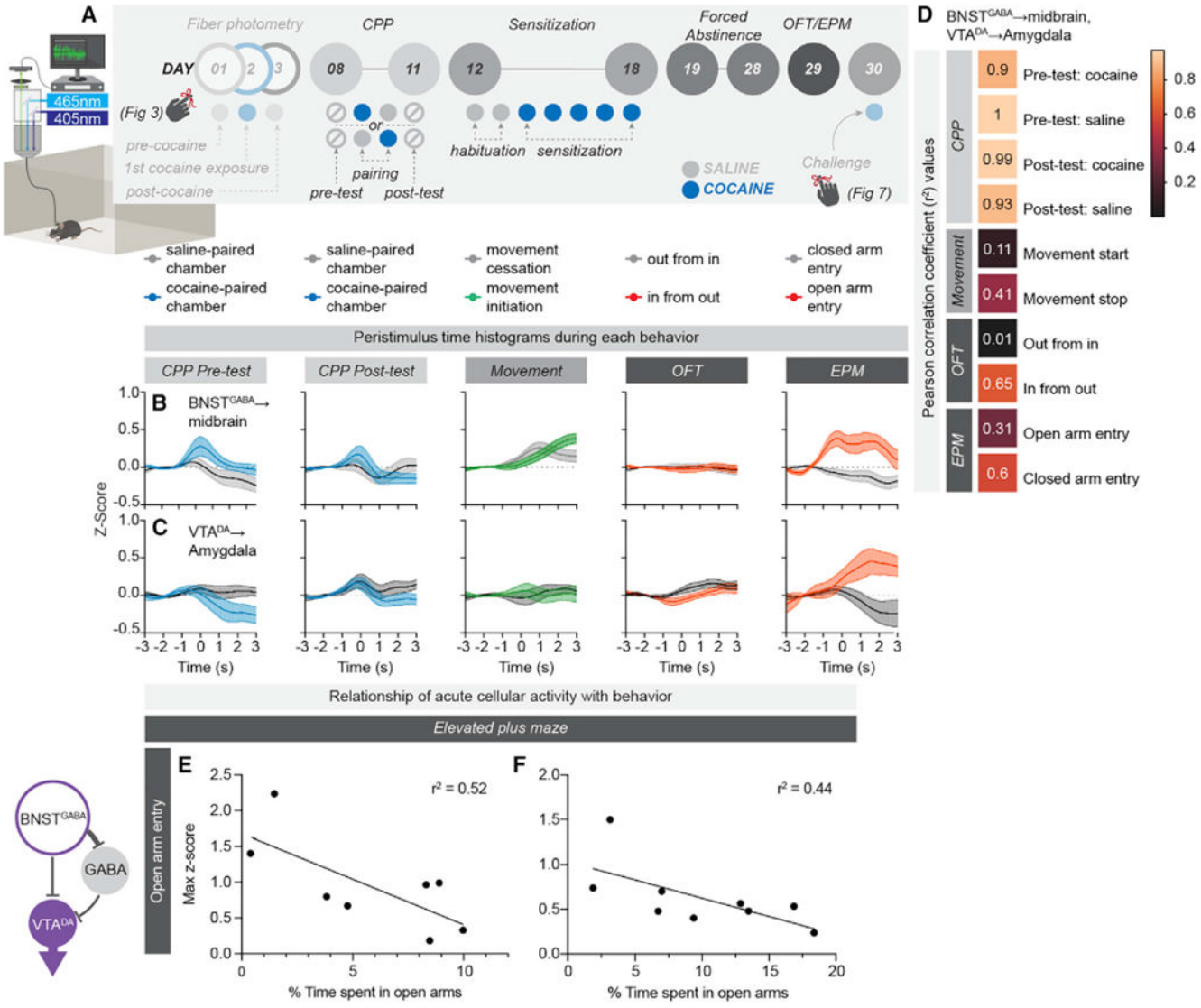

Figure 5. Task-linked cell activity in the BNST^{GABA}→VTA^{DA}→amygdala pathway is related to anxiety behavior

(A) Schematic and timeline of fiber photometry experiments.

(B and C) Peristimulus time histograms (PSTHs) for (B) BNST^{GABA}→midbrain cells and (C)VTA^{DA}→amygdala cells during five different tasks: chamber crossings into the saline-paired and cocaine-paired chamber in the CPP pre-test and CPP post-test, movement initiation and movement cessation in the open field, entering or exiting the center of the open field in the OFT, and entering the open or closed arms of the EPM. n =

(D) Correlogram showing r^2 values for activity for BNST^{GABA}→midbrain cells and VTA^{DA}→amygdala cells in the 0.5 s preceding and 1.5 s after the identified behavioral event.

(E and F) Correlations of maximum *Z* scores in (E) BNST^{GABA} and (F) VTA^{DA}→amygdala cells with time in the open arms of the EPM for each mouse (n = 8 for BNST^{GABA}, 9 for VTA^{da}→amygdala).

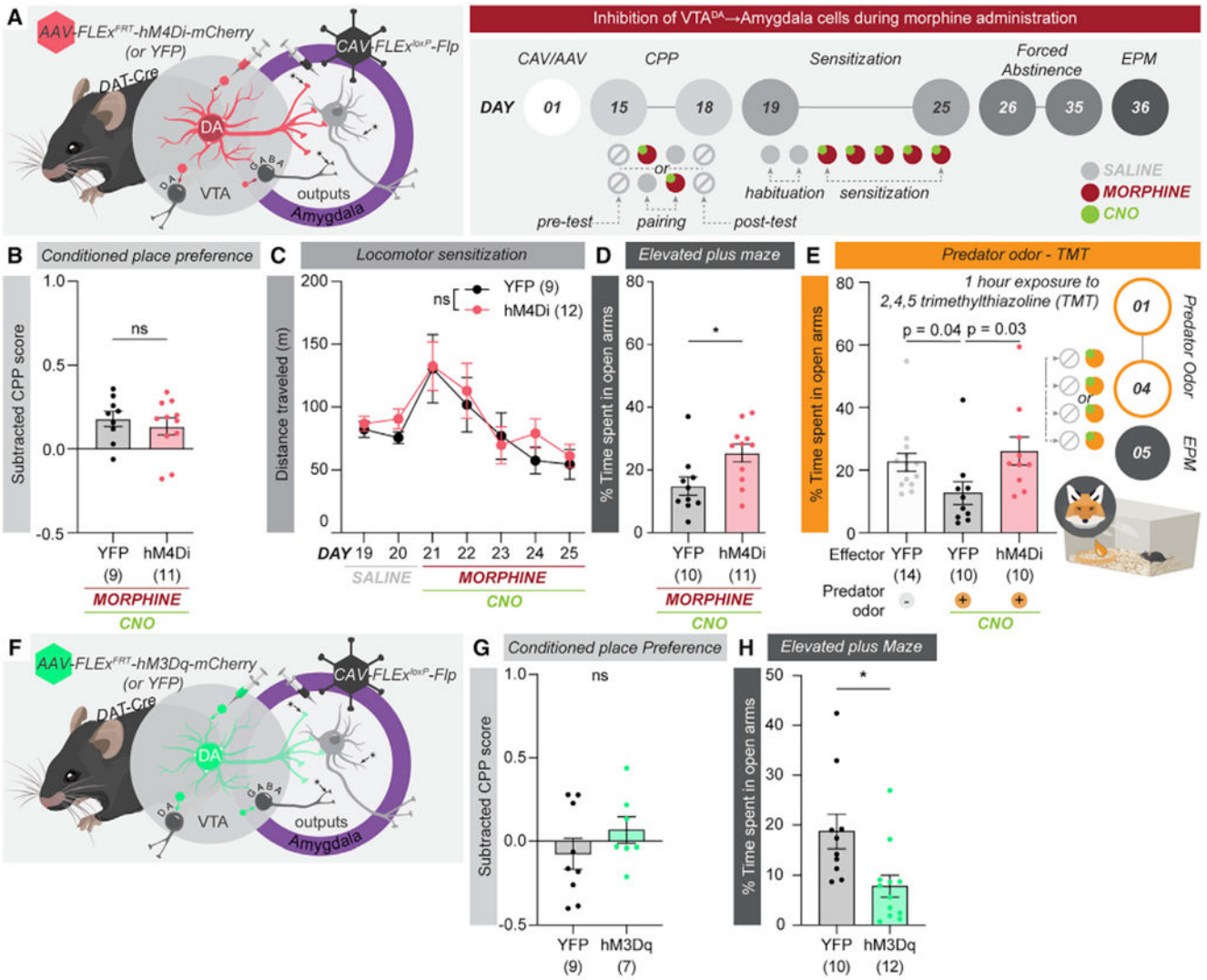

Figure 6. VTA^{DA}→amygdala cell activity is generally required for development of experience-dependent anxiety states

. (A) Schematic and timeline of VTA^{DA}→amygdala cell inhibition.

(B–D) Inhibition of VTA^{DA}→amygdala cells had no effect on CPP (YFP versus hM4Di, p = 0.52; n = 9 YFP, 11 hM4Di) (B) or locomotor behavior (YFP versus hM4Di, 2-way ANOVA, p = 0.34; n = 9 YFP, 12 hM4Di) (C) but did prevent development of anxiety (YFP versus hM4Di, p = 0.02; n = 10 YFP, 11 hM4Di) (D).

(E) Inhibiting VTA^{DA}→amygdala cells prevented anxiety that developed after chronic exposure to TMT (YFP/no predator odor (PO) versus YFP/PO, p = 0.04; YFP/PO versus hM4Di/PO, 0.03; YFP/no PO versus hM4Di/PO, p = 0.49; n = 14 YFP/no PO, 10 YFP/PO, 10 hM4Di/PO).

(F) Strategy for chemogenetic excitation of VTA^{DA}→amygdala cells.

(G) A single pairing of CNO did not cause a place preference or place aversion (YFP versus hM3Dq, p = 0.28; n = 9 YFP, 12 hM3Dq).

(H) hM3Dq-mediated activation of $VTA^{DA}\rightarrow$amygdala cells induced anxiety-like behavior (YFP versus hM3Dq, $p = 0.012$; $n = 10$ YFP, 12 hM3Dq).

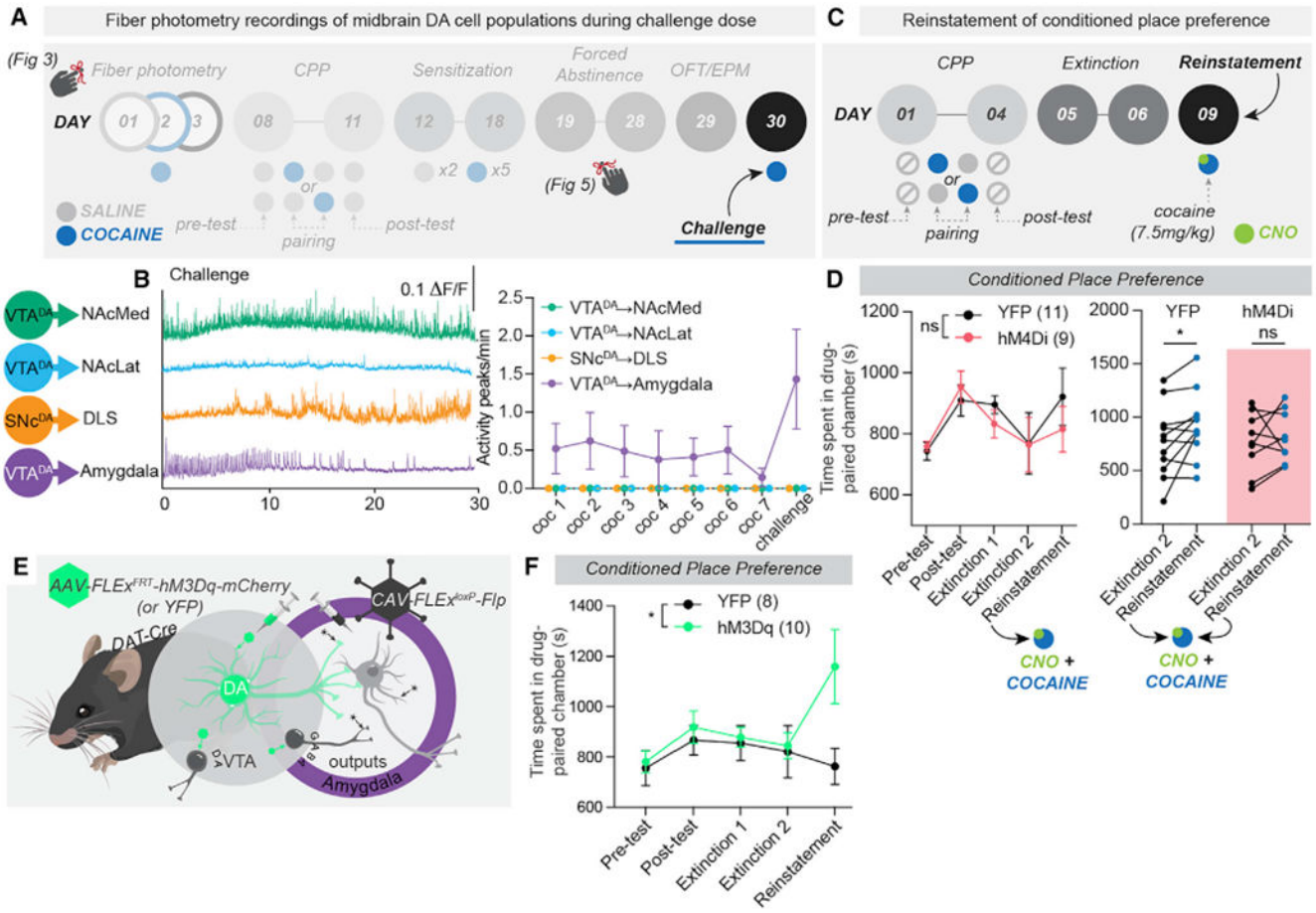

Figure 7. Activity in VTA^{DA}→amygdala cells is necessary and sufficient for reinstatement of cocaine CPP.

(A) Timeline for fiber the photometry experiments. Mice were the same as those used for Figure 5.

(B) Representative traces from each of four midbrain DA cell populations in response to a challenge dose of cocaine after 10 days of forced abstinence. The frequency of rhythmic peaks for all cell populations during the first 10 min after each cocaine dose was quantified. n = 10 VTA^{DA}→NAcMed, 10 VTA^{DA}→NAcLat, 11 SNc^{DA}→DLS, 9 VTA^{da}→amygdala.

(C) Timeline for the CPP reinstatement experiments.

(D) Inhibiting VTA^{DA}→amygdala cells during the priming dose prevented cocaine-induced CPP reinstatement (before/after YFP, p = 0.04; hM4Di, p = 0.57; n = 11 YFP, 9 hM4Di).

(E) Strategy for chemogenetic excitation of VTA^{DA}→amygdala cells.

(F) Chemogenetic excitation of VTA^{DA}→amygdala cells during the reinstatement testing strongly reinstated the preference for the cocaine-paired side (2-way ANOVA, p = 0.04; n = 8 YFP, 10 hM3Dq).

KEY RESOURCES TABLE

REAGENT or RESOURCE	SOURCE	IDENTIFIER
Antibodies		
Chicken anti-GFP	Aves Labs	Cat# GFP-1020, RRID:AB_10000240
Rabbit anti-TH	EMD Millipore	Cat#AB152, RRID:AB_390204
Rat anti-mCherry mAb	ThermoFisher	Cat#M11217, RRID:AB_2536611
Donkey anti-chicken AlexaFluor488	Jackson ImmunoResearch	Cat# 703-545-155, RRID:AB_2340375
Donkey anti-rat Cy3	Jackson ImmunoResearch	Cat# 712-165-153, RRID:AB_2340667
Donkey anti-rabbit AlexaFluor 647	Molecular Probes	Cat# A-31573, RRID:AB_2536183
Bacterial and virus strains		
AAV_5-CAG-FLEx^{FRT}-TC	University of North Carolina, vector core	N/A
AAV_8-CAG-FLEx^{FRT}-RABV-G	University of North Carolina, vector core	N/A
AAV_{DJ}-hSyn-FLEx^{FRT}-hM4Di	University of North Carolina, vector core	N/A
AAV_{DJ}-hSyn-FLEx^{FRT}-hM3Dq	Gene Vector and Virus Core lab at Stanford University	N/A
AAV_{DJ}EF1 α-fDIO-eYFP	University of North Carolina, vector core	N/A
AAV_5-EF1 α-fDIO-GCaMP6f	Gene Vector and Virus Core lab at Stanford University	N/A
AAV_{retro}-EF1 α-fDIO-Cre	Addgene	Cat121675-AAVrg
AAV_1hSyn-FLEx^{loxP}-jGCaMP7f	Addgene	Cat#104488-AAV1
AAV_8-hSyn-FLEx^{FRT}-mGFP-2A-Synaptophysin-mRuby	University of North Carolina, vector core	N/A
CAV-FLEx^{loxP}-Flp	Plateforme de Vectorologie de Montpellier, France	N/A
RABV▵DG	This paper	N/A
Chemicals, peptides, and recombinant proteins		
Cocaine hydrochloride	Sigma	Cat#C5776-1G; CAS:53-21-4
Morphine	Patterson Veterinary	Cat#78924699
Clozapine-N-oxide (CNO)	Hello bio	Cat#HB1807
Degradex PLGA CNO microspheres	Phosphorex	Cat#LG1000-CNO
2,4,5 trimethylthiazoline (TMT)	BioSRQ	Cat#1G-TMT-90
Paraformaldehyde	Sigma	Cat#P6148; CAS: 30525-89-4
Triethanolamine	Sigma	Cat#T58300; CAS: 102-71-6
Acetic anhydride	Sigma	Cat#242845; CAS: 108-24-7
Formamide	Sigma	Cat#47671-1L-F; CAS: 75-12-7
Dextran sulfate	Sigma	Cat#D8906; CAS: 9011-18-1
Tween-20	Sigma	Cat#P9416; CAS: 9005-64-5
Deposited data		
Fiber photometry recording	This paper	Zenodo: https://doi.org/10.5281/zenodo.6415883

REAGENT or RESOURCE	SOURCE	IDENTIFIER
RABV tracing data	This paper	Zenodo: https://doi.org/10.5281/zenodo.6415883
Experimental models: Organisms/strains		
Mouse B6.SJL-*Slc6a3*$^{tm1.1(cre)Bkmn}$/J (DAT-Cre)	The Jackson laboratory	RRID:IMSR_JAX:006660
Mouse Slc32a1-2A-FlpO-D knock-in (vGAT-Flp)	The Jackson laboratory	RRID:IMSR_JAX:029591
Oligonucleotides		
See Table S1 for the list of probes for FISH	This paper	N//A
Clean G	This paper	N/A
REAGENT or RESOURCE	SOURCE	IDENTIFIER
Oligo imager	This paper	N/A
42 bp hairpin sequence	This paper	N/A
Software and algorithms		
Imaris	Bitplane	N/A
MATLAB	MathWorks Inc	N/A
Prism 9	GraphPad https://www.graphpad.com/scientific-software/prism/	N/A
Fiji	https://imagej.net/software/fiji/?Downloads	N/A
Biobserve	http://www.biobserve.com/	N/A
Python 3.8	https://www.python.org/downloads/release/python-380/	N/A
MATLAB script for FP analysis	This paper	Zenodo: https://doi.org/10.5281/zenodo.6415661
MATLAB script for PSTH analysis	This paper	Zenodo: https://doi.org/10.5281/zenodo.6415661
Python codes for PSTH analysis	This paper	Zenodo: https://doi.org/10.5281/zenodo.6415661
Other		
Superfrost Plus Micro slides	VWR	Cat#48311-703
Fluoromount-G™	Invitrogen	Cat#00-4958-02
Cover glass	Thermo Scientific	Cat#152460
Optical fiber	THORLABS	Cat#FT400EMT
Vetbond tissue adhesive	Patterson Veterinary	Cat#78055031
Vetameg	Patterson Veterinary	Cat# 07-892-4375
Metal screws	Antrin Miniature Specialists	Cat#AMS90/1B
Metabond	Parkell	Cat#S380
Geristore A	Den-Mat holdings	Cat#4506
Geristore B	Den-Mat holdings	Cat#034523101